Chapter- 4

4.1 Introduction

Commercial endeavors have widely utilized synthetic colors with aromatic azo groups as food additives [1]. Natural dyes that were produced from fruits, plants, and minerals were once employed as food coloring during the pre-industrial era. However, in recent years, synthetic dyes have become a popular coloring additive in a wide range of food products to make up for color loss during preservation, add flavor, and make them appear vivid. Synthetic colorants have a have relatively intense color than natural dyes which appear quite attractive to children, thereby negatively impact children's food preferences in a clandestine manner. And importantly, they are less expensive than natural dyes. Dairy, chilli powder, cold drinks, sugar candies, cakes, and gelatins all contain common color additives such Tartrazine, Sunset yellow, and Sudan dyes [2–4]. Nevertheless, a number of studies show that the misuse of food coloring in food products has negative effects on human health, including hyperactivity problem, pediatric mental illness, and DNA damage, in addition to having toxic and cancer-causing effects on animals [5–6]. The usage of some food dyes, such as Sudan dye, Congo red, rhodamin B, Amaranth, Allura red, Tartrazine, and Sunset yellow, has been outright banned by several governments [7–9]. An Indian case study revealed that legal synthetic colors were improperly applied, and in certain instances, unapproved dyes were being used in food products without authorization [10]. For example, several countries have outlawed the use of Sudan I dye in food products, since it has been identified as a third group genotoxic carcinogen that causes chronic toxicity to humans and animals as well as reproductive toxicity and cancer, despite this, a number of instances involving the usage of Sudan I were documented [11].

Because color is a vital component in food items and chilli powder is one of them, the prevalence of food fraud is drastically rising as the food supply chain becomes more global. As a result, fake chilli powder is being produced and artificial colors are being added to chilli powder to change its natural color [12]. Since India is the largest producer, consumer, and exporter of chilli in all of South Asia, as well as in the U.K. and China, Sudan I was recognized in hot chilli items imported from India [13].

Therefore, it is crucial to establish a reliable analytical technique for the non-invasive, label-free detection of these synthetic dyes. To identify the adulteration of these colors in food stuffs or chilli powder, several analytical tests have been implemented, such as liquid chromatography mass spectrometry (LC-MS), chromatography, enzyme-linked immune sorbent assays, high performance liquid chromatography (HPLC), thin layer chromatography (TLC), etc. [1, 14–16]. These, traditional analytical techniques take a long time, endure a challenging sample preparation process, and are typically not suitable to detect in situ or rapid assessment. Among these methods surface enhanced Raman spectroscopy has emerged as a promising analysis tool for the detection of dyes in food due to its great sensitivity and quick detection potential [9, 17–18]. SERS's high sensitivity is typically controlled by two processes as chemical enhancement, a weaker process (EF~ 10^3) typically attributed to the charge transfer between the substrate and analyte molecule, and an enhanced electromagnetic field caused by the excitation of a localized surface plasmon resonance (LSPR) when the probe molecule comes into contact with coinage metal substrates like gold, silver, and copper [19, 20]. Bismuth oxyhalides (BiOX = I, Br, Cl) drawn a lot of interest, which are increasingly exploited in photo-

catalysis and environmental remediation because to their strong catalytic performance, distinctive layering, and band structure, due to its broad band gap, BiOBr is an active nanomaterial primarily in the ultraviolet (UV) region [21]. To boost the efficiency of using BiOBr, its optical quality must be expanded to the visible light range. In a variety of applications, including photocatalysis, photovoltaic devices, using bismuth oxyhalides as a substrate in SERS fields, etc., noble metals have been extensively exploited to enhance the optical properties and provide new functions. Silver nanoparticles are readily oxidized due to their poor chemical stability because it is difficult to use in acidic or heating condition. This can be overcome by making the nanoparticles from various composite materials [21–24]. Numerous semiconducting-plasmonic composites such as Ag/TiO2, ZnO/Ag etc., displayed high SERS [25–26]. In this regard, we utilized a combination of bismuth oxybromide with noble metal to examine the SERS performance for the detection of toxic dyes.

In this work, the CTAB assisted-BiOBr, $Ag_{0.09}$BOB or $Ag_{0.15}$ BOB (CTAB-AgBr-Bi_3O_4Br/BiOBr) substrates were synthesised and used as novel SERS substrate. The SERS activity was performed by using Rhodamin 6G (R6G) as a proof of principle. Further, SERS substrate was used to analyse the food colors such as Allura red (AR), Amaranth (AM), Tartrazine (TR) and Sunset yellow (SY), hitherto unreported to the best of our knowledge. In addition, the potential of the prepared SERS substrate simultaneous detection of binary solutions of food colors were demonstrated. In the subsequent part, Bismuth oxybromide and silver containing BiOBr substrates were tested for its SERS activity in situ detection of adulterated chilli powder in different solvents acetonitrile,

methanol, and acetone. To compare the constituent present in chilli powder some chilli fruits and their seeds were also analysed.

4.2 Experimental section

4.2.1 Materials

$AgNO_3$, CTAB (cetyltrimethylammonium bromide), Rhodamine 6G (Merck), Sudan I (Tokyo Chemical Industry India Pvt. Ltd. or TIC), NaOH, ethanol, acetylcholine, methanol (Merck) were purchased and used without any processing. Food colours like Amaranth, Allura red (SRL, India), Tartrazine and Sunset yellow were purchased from the local market in Varanasi, India. Double distilled water was used throughout. Three different brands of chilli powder and five different types of chilli fruits were bought from the local market in Varanasi, India.

4.2.2 Synthesis of CTAB-AgBr-Bi_3O_4Br/BiOBr

Chemical precipitation method was used to synthesize CTAB-AgBr-Bi_3O_4Br/BiOBr. Briefly, in 15 mL of 1.5 M dil.HNO_3, 0.11M of Bi $(NO_3)_3.5H_2O$ was dissolved. With vigorous stirring, 2 ml of an aqueous solution containing two different concentrations of $AgNO_3$ (0.09 mmol and 0.15 mmol) were simultaneously added into bismuth solution. Afterwards, drop-wise additions 0.69 mmol of CTAB in 40 mL of aqueous 9.3 mmol NaOH were added to the aforementioned acid solution while it was being vigorously magnetically stirred at room temperature. After 1.5 hours of stirring, the white precipitate was collected, thoroughly washed three times in distilled water and ethanol, and then dried in oven for overnight at 100 ^{o}C to produce to obtain CTAB-AgBr-Bi_3O_4Br/BiOBr.

Additionally, the same process was used to prepare CTAB assisted-BiOBr without $AgNO_3$. The substrates were labeled as BOB (CTAB assisted-BiOBr), $Ag_{0.09}$BOBor $Ag_{0.15}$BOB (CTAB-AgBr-Bi_3O_4Br/BiOBr).

4.2.3 Characterization

Synthesized samples were characterized by various techniques explained in chapter 1 section 1.6.

4.2.4 Raman Measurement

The SERS activity of the novel bismuth-based substrate was evaluated using five distinct molecules as food colorants such as R6G, AR, AM, TZ, and SY. R6G was dissolved in ethanol to prepare a series of solutions from1mM to 10 µM. Other dyes were produced in aqueous solution with concentrations ranging from 1 mM to 40 µM. 100 µl of analyte solution were added to microparticle substrates and kept for 2h, after that mixed solution was dropped onto a glass slide and dried at room temperature before the SERS measurements. Raman and SERS activity measurement of substrate was conducted under a laser power of 80 mW. SERS spectra of R6G, AR and AM were recorded with integration time of 8 s. The SERS signals of TR and SY were collected with laser power of 80 mW and exposure time of 15 s.

4. 3 Results and Discussion

4.3.1 XRD pattern

By using X-ray diffraction (XRD), the crystal plane of CTAB assisted-BiOBr and theCTAB-AgBr-Bi_3O_4Br/BiOBr were characterized. The XRD pattern of the CTAB-assisted-BiOBr is shown in **Figure 4.1**, which displays the diffraction peaks of BiOBr at 2θ values (in degree) at 21.88, 25.22, 31.76, 32.28, 33.20, 34.06, 39.34, 44.36, 46.28, 50.7, 57.22, 76.86 which correspond to the indices (002), (011), (012), (110), (003), (111), (112), (004), (020), (014), (212) planes of tetragonal BiOBr (JCPDS no. 73-2061). In addition, adding a silver source affects the crystal structure of BiOBr. As silver source increases from $Ag_{0.09}$BOBto $Ag_{0.15}$BOB, the diffraction peaks of AgBr and BiOBr increases, while the peaks of Bi_3O_4Br decreases. This indicates that stability of composite material increases as concentration of silver increases. In situ growth of AgBr with the characteristic diffraction peaks appeared at 26.76, 30.96, 44.36, 55.04, 64.48, 73.26, were assigned to the planes (111), (200), (220), (222), (400), (420) (JCPDS no. 06-0438) and new diffraction peaks appeared at (112), (114) which can be attributed to Bi_3O_4Br (JCPDS no.84-0793) as shown in **Figure 4.1 (b-c)**. The observed results reveal the formation of composite materials.

The average crystalline size of BOB, $Ag_{0.09}$BOB and $Ag_{0.15}$BOB materials were calculated to be 10.1, 40.8, and 30.4 nm, using the Scherrer equation [27].

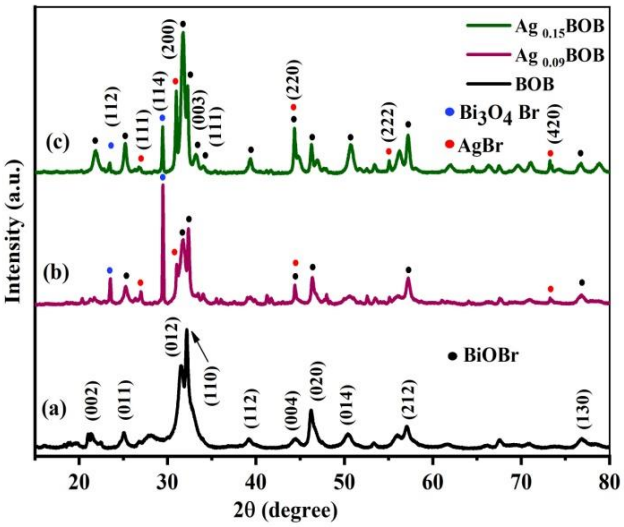

Figure 4.1 *XRD pattern of (a) CTAB assisted-BiOBr (BOB) (b) $Ag_{0.09}$BOB (c) $Ag_{0.15}$ BOB.*

4.3.2 UV-Visible spectra

UV-visible spectroscopy was used to examine the optical properties of BOB, CTAB-AgBr-Bi_3O_4Br/BiOBr with different silver compositions, including$Ag_{0.09}$BOB and $Ag_{0.15}$ BOB. The UV-visible absorbance spectra of these substrates reveal two distinct absorption bands at 260 and 355 nm in $Ag_{0.09}$BOB and $Ag_{0.15}$ BOB compared to BOB, which confirm the presence of silver as shown in **Figure 4.2**. The dipole resonance of silver is responsible for the band at 355 nm, and the absorption band at 260 nm is due to BiOBr [28].

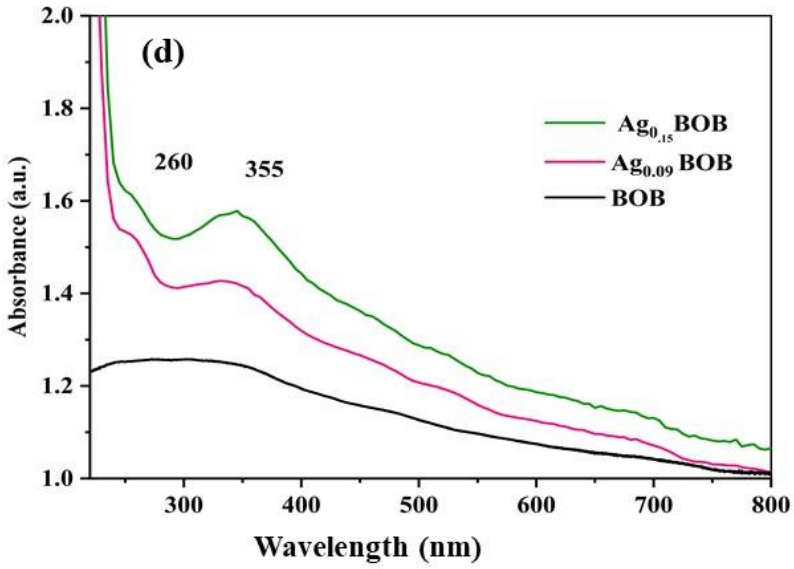

***Figure 4.2** UV-visible spectra of BOB, $Ag_{0.09}$BOB, and $Ag_{0.15}$BOB.*

4.3.3 SEM analysis

Scanning electron microscope (SEM) was employed to characterize the surface morphology of the prepared samples, as shown in **Figure 4.2**. **Figure 4.2 (a)** depicts the flake-like structure of CTAB assisted-BiOBr with an average size of 0.6-0.8 µm. **Figure 4.2 (b)** shows the flake and rod-like structure of $Ag_{0.09}$BOB (CTAB-AgBr-Bi_3O_4Br/BiOBr) microparticles with average length of 0.55-0.65 µm and 3.2-3.4 µm, respectively. **Figure 4.2 (c)** shows the aggregated flake and rod-like structure (with different magnifications in **Figure 4.2 (c')**) of $Ag_{0.15}$BOB (CTAB-AgBr-Bi_3O_4Br/BiOBr) microparticles with length of 0.50-0.55 µm and 2-3.3 µm. The outcome indicates that after the addition of the silver source morphology is changed.

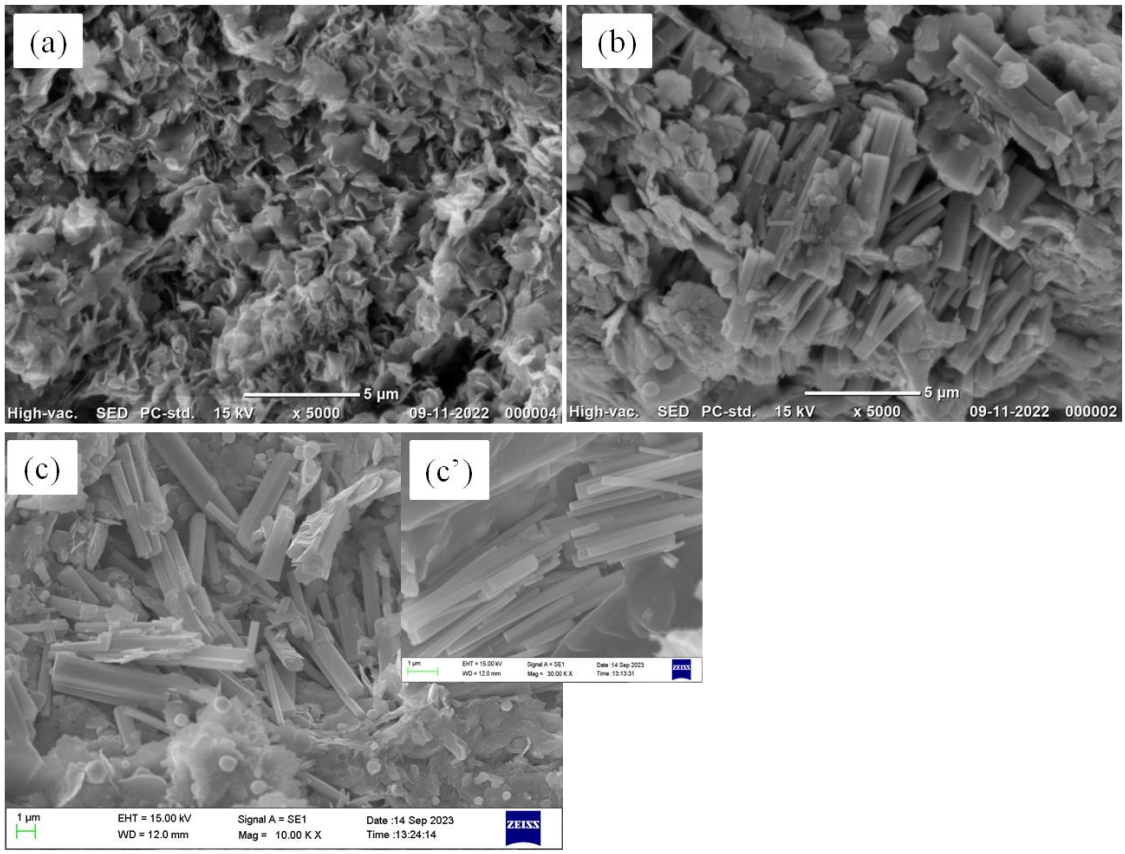

Figure 4.3 *SEM image of (a) CTAB assisted-BiOBr (BOB) (b) CTAB-AgBr-Bi_3O_4Br/BiOBr ($Ag_{0.09}$BOB) (c) and (c') $Ag_{0.15}$ BOB.*

4.3.4 XPS analysis

The surface composition and chemical state of $Ag_{0.09}$BOB composite was analysed by XPS (**Figure 4.4**). The survey spectrum demonstrates that microparticles contain Ag, Bi, O and Br (**Figure 4.4 (A)**). There is an adventitious Carbon species peak at a binding energy of 285.08 eV [29] (**Figure 4.4 (A)**). The high-resolution spectrum is shown in **Figure 4.3 (B)** in which Bi 4f consist of two peaks at 158.6 and 163.9 eV corresponds to Bi $4f_{7/2}$ and Bi $4f_{5/2}$ respectively, which confirmed the presence of Bi^{3+} state in BiOBr [30]. **Figure 4.4 (C)** shows the XPS spectrum of O1s, the dominant peaks

at 529.5 eV and 531.7 eV can be attributed to lattice oxygen in Bi-O-Br and surface adsorbed components of hydroxyl group respectively [29].The Br 3d spectrum in **Figure 4.4 (D)** displays peaks at 67.7 and 68.7 eV corresponding to Br $3d_{5/2}$ and Br $3d_{3/2}$, which showed the presence of Br^{-} in AgBr and BiOBr [22]. **Figure 4.4 (E)** shows the XPS spectrum of Ag 3d at binding energies 367.2 and 373.1 eV are assigned to Ag $3d_{3/2}$ and Ag $3d_{5/2}$confirm the presence of Ag^{+} ion in $Ag_{0.15}$BOB composite [23], [30]. Further, the obtained results are in accordance with the XRD findings.

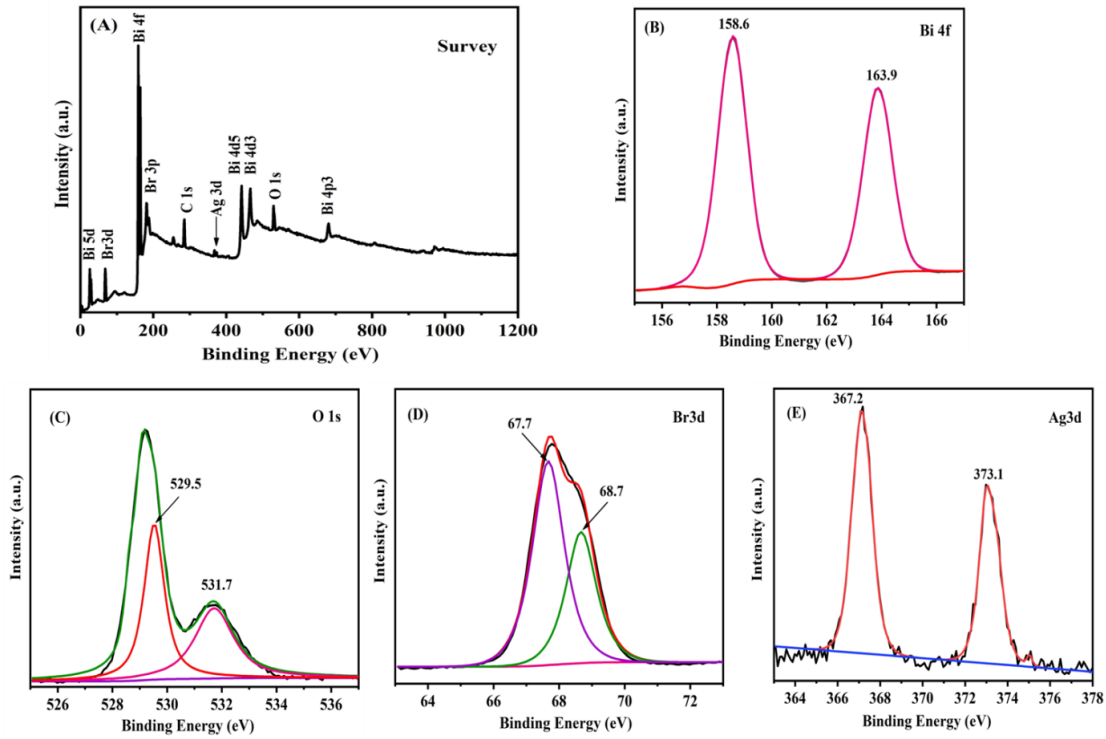

Figure 4.4 *XPS spectrum of $Ag_{0.15}$BOB (CTAB- AgBr- Bi_3O_4Br/BiOBr) (A) survey spectrum and high resolution spectrum for (B) Bi 4f, (C) O 1s, (D) Br 3d, (E) Ag 3d.*

4.3.5 FTIR Analysis

FTIR analysis was carried out to identify the different functional groups present in the prepared composites and to show the appearance of the peaks in all samples for comparison. The presence of CTAB on the surface of BiOBr was confirmed by FTIR analysis as shown in **Figure 4.5**. The broad band at 3429 and 1629 cm^{-1} may be attributed to the stretching vibration of –OH group and bending H–O–H respectively, the increased broadness in $Ag_{0.09}$BOB and $Ag_{0.15}$BOB arises due to adsorbed H_2O on the surface of AgBr [31–32]. As shown in Figure 4.5 of $Ag_{0.15}$ BOB, the intensity of peaks at 2849, 2917 $cm^{-1}$are weaker than those of CTAB assisted-BiOBr (BOB) are caused by the symmetric and asymmetric stretching vibration mode of methyl and methylene groups of CTAB, respectively [32]. The most intense peaks at 1384, and 1467 cm^{-1} arises due toasymmetric and symmetric C-H scissoring vibration of N^+-CH_3 [33–34]. The observed peak at 720 cm^{-1}can be assigned to rocking mode of methylene chain and the peaks at 814, 909, 962, 1034 cm^{-1} can be attributed to C-N^+ stretching bands [32]. The peak at 524 cm^{-1} can be assigned to the Bi-O stretching vibration of BiOBr [33]. The new peak appeared at 825 cm^{-1}(shown as inset in **Figure 4.5**) in $Ag_{0.09}$BOB and $Ag_{0.15}$BOB may be attributed due to the C-Br stretching bond [29], which did not appear in the spectrum of BOB. These results suggest that CTAB exist at the surface of silver containing bismuth composites.

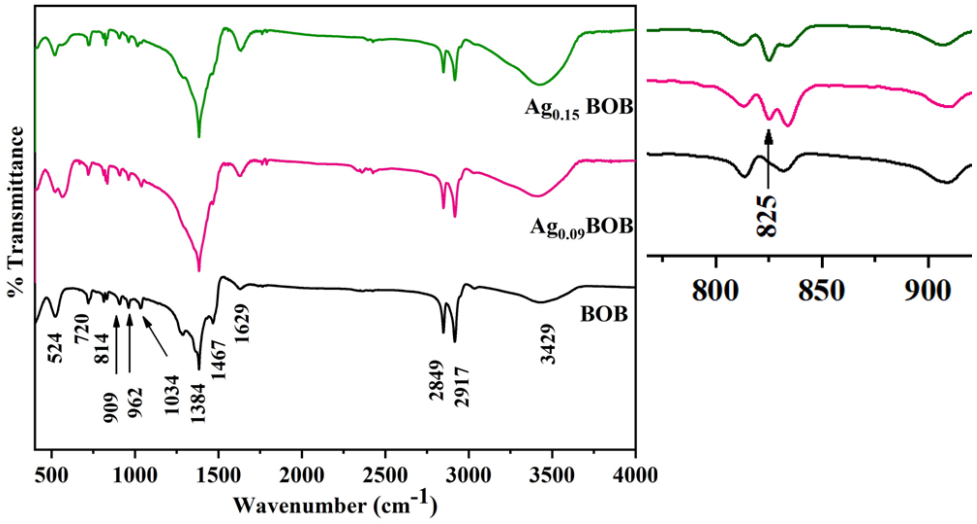

Figure 4.5 *FTIR spectra of BOB, $Ag_{0.09}$BOB, and $Ag_{0.15}$BOB.*

4.3.6 Raman study of CTAB-AgBr-Bi_3O_4Br/BiOBr

Figure 4.6 (a) and **(b)** shows the Raman spectra of pure solid CTAB and CTAB adsorbed on bismuth-based composites, respectively. As shown in **Figure 4.6 (b)**, CTAB assisted-BiOBr (BOB) composite showed Raman signal at 756, 957, 1042, 1130, 1297, and 1449 cm^{-1}. The shoulder peaks at 756 and 957 cm^{-1} were attributed to both CH_3 rocking and C-N^+ stretch. Blue shift at 1042 by 11 cm^{-1} and 1449 cm^{-1} by 18 cm^{-1} in Raman spectrum of CTAB assisted bismuth composites as compared to pure solid Raman spectrum of CTAB, was due to C-C stretching and due to the combination of CH_2 scissors, and CH_3 deformation, which demonstrates the interaction of CTAB with bismuth composites. After the introduction of AgBr the vibrational signals of CTAB significantly decreased. This result suggests that CTAB dissociated from metal surface in the presence of AgBr and revealed the adsorption of CTAB on the surface of silver containing bismuth composites, which corroborated well with the FTIR analysis. Composites $Ag_{0.09}$BOB or

$Ag_{0.15}$BOB demonstrated the characteristic Raman modes of CTAB at 1042, 1130, 1297, 1449 cm^{-1}. The most prominent Raman band at 1042 cm^{-1} corresponds to C-C stretch. The Raman peaks at 1130, 1297 and 1449 cm^{-1} were due to C-C stretching, CH_2 twist, and due to the combination of CH_2 scissors, and CH_3 deformations, respectively [34].

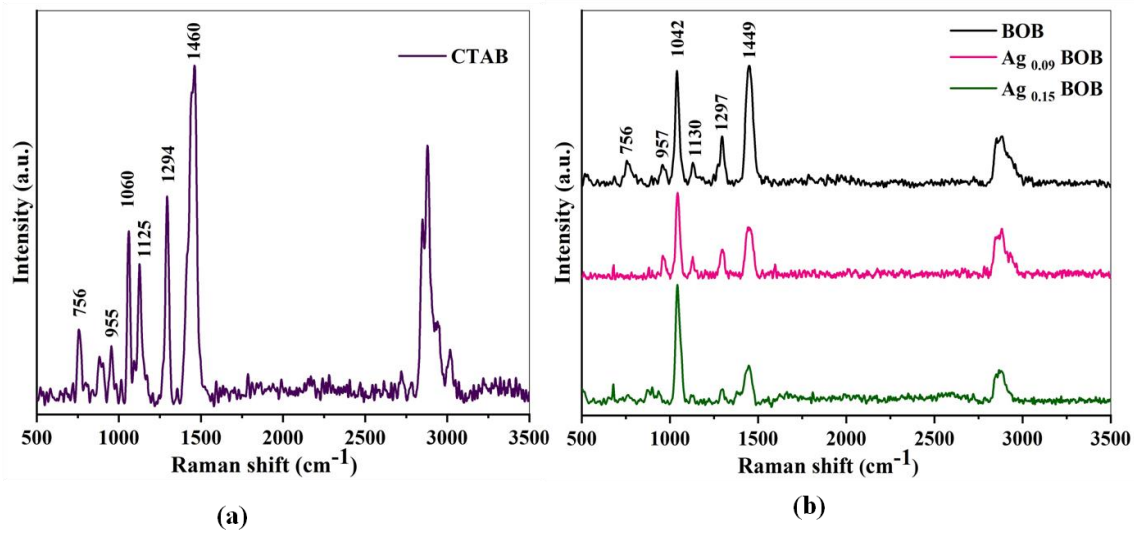

Figure 4.6 *(a) Raman spectra of pure CTAB and (b) Raman spectra of BOB, $Ag_{0.09}$BOB and $Ag_{0.15}$BOB composites.*

4.3.7 SERS study of the prepared composites

Ethanolic solution of R6G was used as a standard probe molecule to preliminarily investigate the SERS activity of the substrate. The SERS activity was performed by mixing 100 µL of R6G solution with substrate BOB (CTAB assisted-BiOBr), $Ag_{0.09}$BOB or $Ag_{0.15}$BOB via comparison of solid and aqueous Raman spectrum.

The SERS activities of BOB, $Ag_{0.09}$BOB or $Ag_{0.15}$ BOB substrates were investigated by using R6G dye with the laser of 785 nm Wavelength. The characteristic

Raman peaks of R6G in solid Raman spectra, shown in Figure 4.7(a) were observed at 607, 768, 1117, 1179, 1302, 1360, 1504, 1559, 1593 and 1664 cm^{-1}, and tentative assignments of these vibrational modes are summarized in Table 4.1. The SERS activity was determined with the detection limit at 100 μM for BOB and $Ag_{0.09}$BOB substrate as shown in **Figure 4.7 (b)**, which indicates that $Ag_{0.15}$ BOB has enhanced SERS activity compared to BOB, and $Ag_{0.09}$BOB.

The SERS spectrum of the probe with varying concentrations of R6G on $Ag_{0.15}$ BOB is shown in **Figure 4.7(c)**. In the SERS spectrum, the intense peaks at 1507, and 1364 cm^{-1} correspond to the C-C stretching mode, while the peak at1305 cm^{-1} was assigned to the N-H in-plane bending mode. The peak at 1194 cm^{-1} due to in plane bending mode of C-H was blue shifted by 15 cm^{-1} [35–36]. The detection limit of R6G on $Ag_{0.15}$ BOBbismuth composite substrate was 10 μM.

Moreover, the most prominent peak at 1507 cm^{-1} of R6G was used in the calibration plot as shown in **Figure 4.7 (d)**. A good linear response was obtained between the SERS intensity and the logarithmic concentration of R6G in the range of 100 μM to 10 μM with the correlation coefficient of $R^2 = 0.980$. The linear equation can expressed as: Raman Intensity (I_{SERS}) = 2470 Log (R6G) + 13139 (4.1)

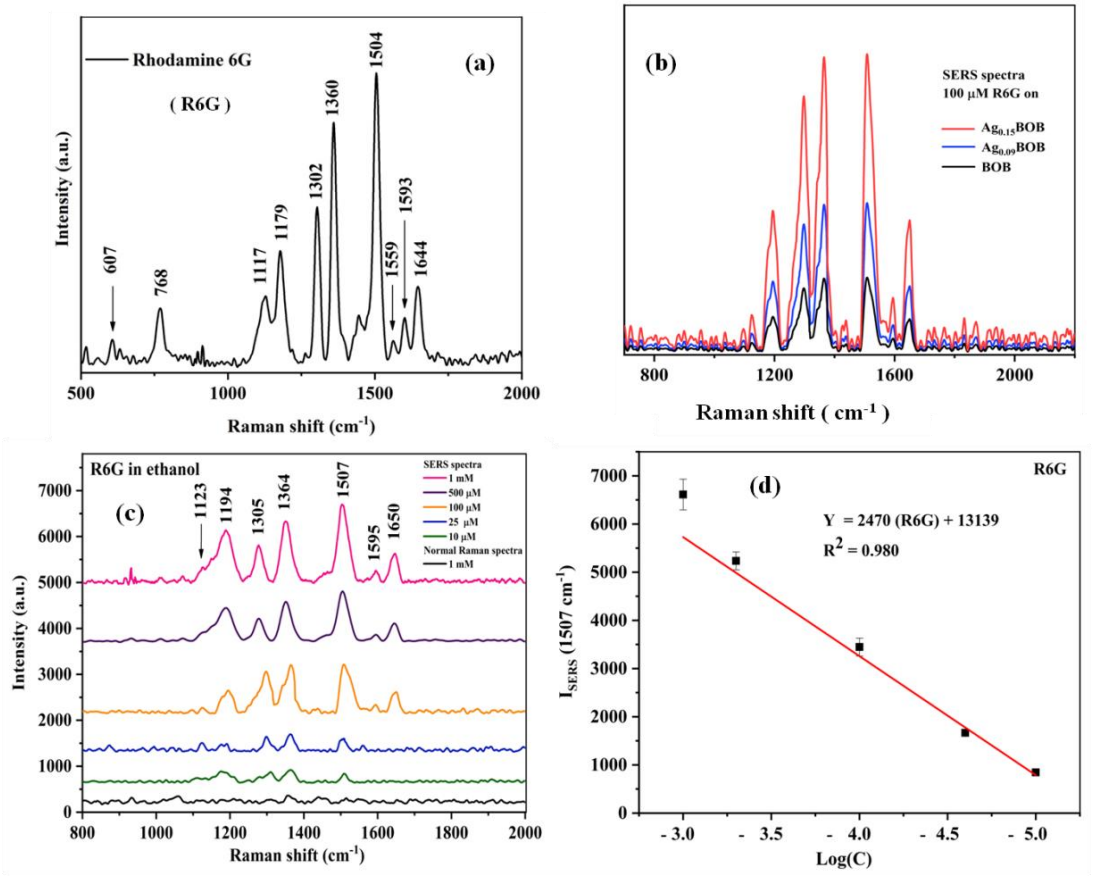

Figure 4.7*(a) Raman spectra of solid Rhodamine 6G (R6G) (b) SERS spectra of 100 µM R6G on BOB, $Ag_{0.15}$ BOB, and $Ag_{0.15}$ BOB (c) SERS spectra of R6G on $Ag_{0.15}$ BOB substrate (100 µM to 10 µM) (d) calibration plot of R6G between intensity and logarithmic concentration of R6G.*

In addition, four different food colours AR, AM, TR, and SY dyes were analysed using $Ag_{0.15}$BOB substrates. Further, normal Raman spectra of solid and aqueous solution of colorants at 1mM concentration were recorded to compare the peak position in the SERS spectrum.

AR is a strongly water soluble azo dye used for coloring food products. **Figure 4.8 (a)** shows the solid Raman spectrum of AR at 751, 974, 1129, 1188, 1223,

1266, 1326, 1383, 1407, 1496, 1578 and 1604 cm^{-1} and their assignment are listed in **Table 4.1**. **Figure 4.8 (b)** shows the SERS spectrum of AR dye on $Ag_{0.15}$BOB substrate, revealing the observed characteristic peaks at 971, 1121, 1190, 1227, 1271, 1316, 1383, 1411, 1491, and 1577 cm^{-1} which is consistent with the solid Raman spectrum. The most intense peak appeared at 1491 cm^{-1}corresponds to C═C stretching in the benzene ringand the sharp peak at 1316 $cm^{-1}$was red shifted by 10 $cm^{-1}$with respect to the solid Raman spectradue to the interaction of dye with the substrate. The other characteristic peaks at 1190, 1227, 1271 and 1411 cm^{-1} were attributed to the SO_2 asymmetrical stretching vibration, rocking (H-C-H) the C–O plane stretching vibration on the benzene ring, and benzene ring and the rocking vibration of H-C-H respectively [17]. The lowest detection limit for AR was 50 μM.

The calibration plot of AR shows (**Figure 4.8 (c)**) that as concentration decreases the intensity of the Raman peak at 1316 cm^{-1} decreases. The correlation coefficient $R^2 = 0.983$ with the linear equation as follows:

$$\text{Raman Intensity } (I_{SERS}) = 1192 \text{ Log (AR)} + 5534 \qquad (4.2)$$

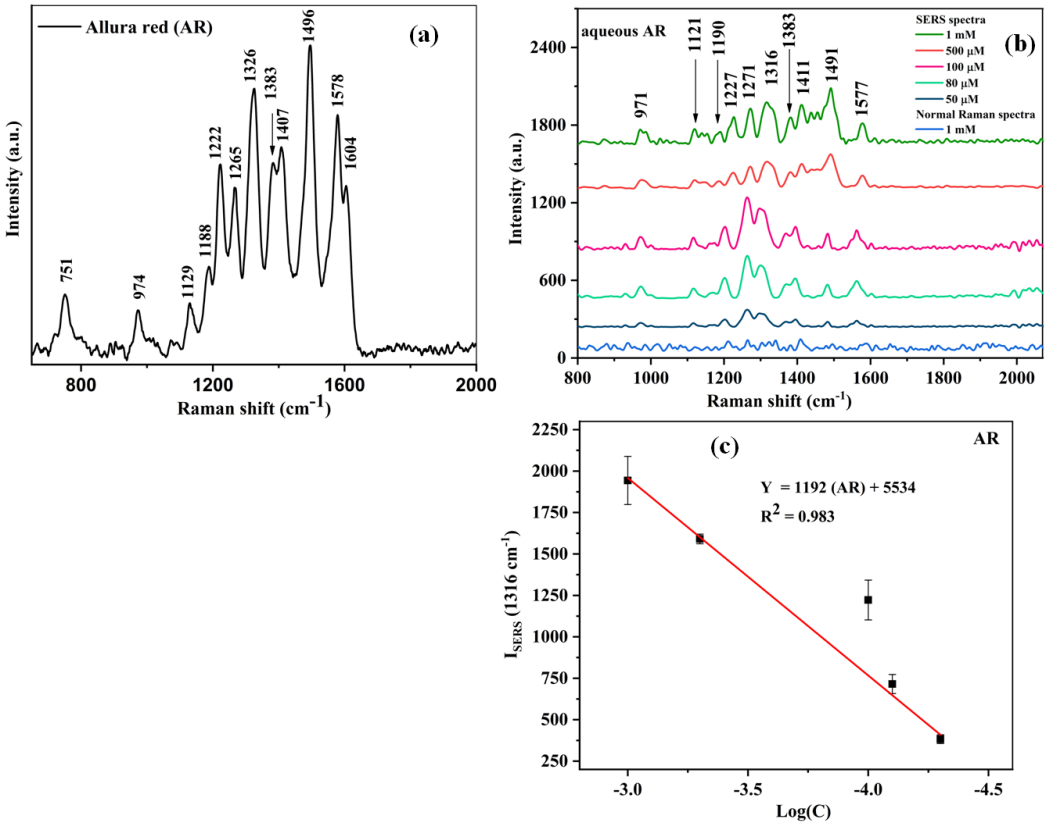

Figure 4.8 *(a) Raman spectra of solid Allura red (AR) (b) SERS spectra of AR (1 mM to 50 µM) on* $Ag_{0.15}$*BOB (c) calibration plot between SERS intensity and logarithmic concentration of AR.*

Figure 4.9 (a) shows the Raman spectrum of AM food color. The characteristic peaks of AM appeared at 738, 1052, 1135, 1172, 1231, 1361, 1401, 1434, 1477, 1511 and 1571 cm^{-1} and their tentative assignments are shown in **Table 4.1**. **Figure 4.9 (b)** shows the SERS spectrum of AM dye acquired on $Ag_{0.15}$BOB substrates, which reveal that the intensity of characteristic Raman peaks decreased with decrease in concentration. The sharp band observed at 1363 cm^{-1} was due to C-C stretching vibration. Another intense Raman bands at 1231, and 1572 cm^{-1} correspond to wagging of O-S, and

asymmetric stretching of ring, respectively, which are in good agreement with the previous report [37–38]. The lowest detection limit of AM was found to be 50 μM.

The most intense peak at 1363 cm^{-1} was used in the calibration plot (**Figure 4.9 (c)**) in the range of 1mM to 50 μM, which demonstrates the increase in intensity with increased concentration. The calibration equation with correlation coefficient $R^2 = 0.972$ is shown below:

Raman Intensity (I_{SERS}) = 5000 Log (AM) + 22482 (4.3)

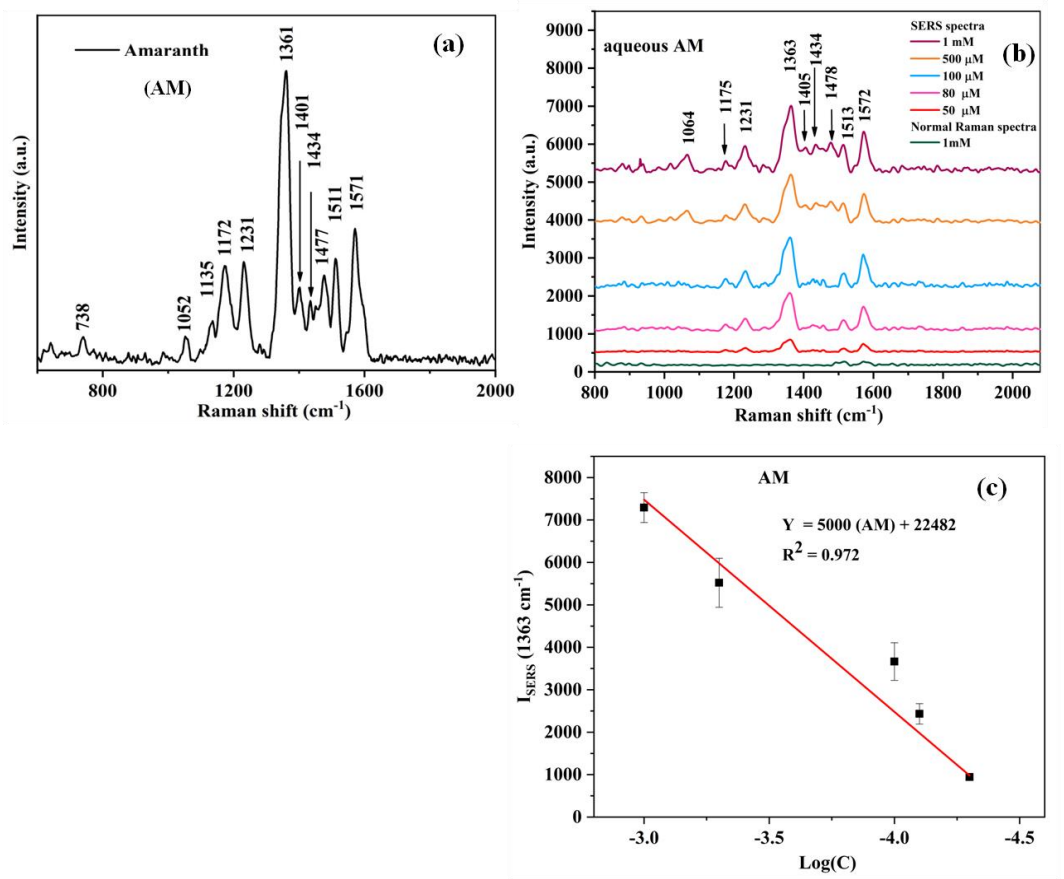

Figure 4.9 *(a) Raman spectra of solid Amaranth (AM) (b) SERS spectra of AM (1 mM to 50 μM)on* $Ag_{0.15}$ *BOB substrate (c) calibration plot between SERS intensity and logarithmic concentration of AM.*

Figure 4.10 (a) show the solid Raman and **Figure 4.10 (b)** shows the SERS spectrum of TR dye on $Ag_{0.15}$BOB substrate. The characteristic Raman peaks of TR were observed at 623, 802, 1044, 1132, 1177, 1217, 1361, 1414, 1499, and 1597 cm^{-1}, and their assignments are listed in Table 4.1 are match well with the previous report [39].

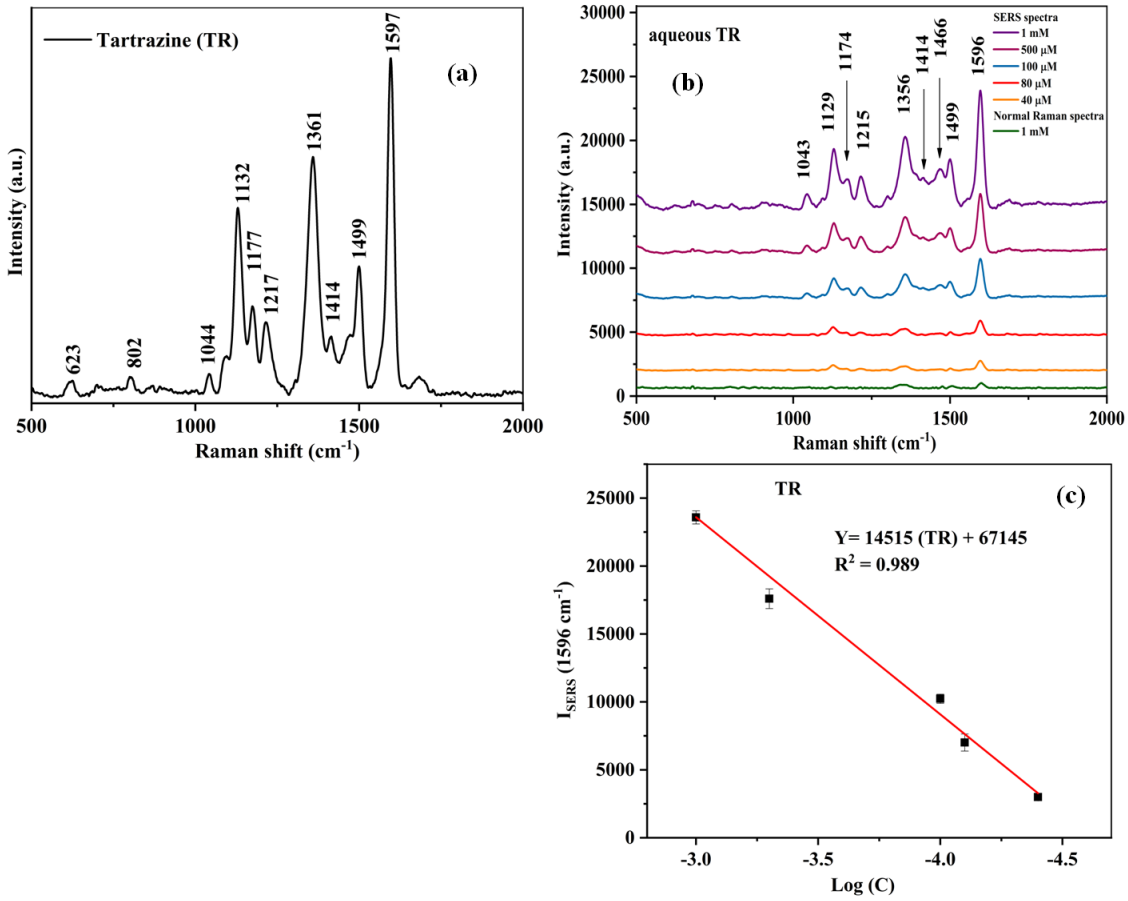

Figure 4.10 *(a) Raman spectra of Tartrazine (TR) (b) SERS spectra of on* $Ag_{0.15}$ *BOB substrate from 1mM to 40 µM, and (c) calibration plot between the SERS intensity and logarithm concentration of TR.*

The most intense peak located at 1596 cm^{-1}in the SERS spectrum corresponds to C-C stretching and C-H wagging in benzene ring and other sharp peaks at 1129, and

1356 cm^{-1} are attributed to N=N stretching, C-H wagging and C-C stretching in naphthalene ring [39]. The lowest detection limit of TR was found to be 40 µM. The peak at 1596 cm^{-1} was selected for quantitative analysis of TR.

The calibration plot (**Figure 4.10 (c)**) demonstrates an excellent linear relation in the range of 1mM to 40µM with the correlation coefficient $R^2 = 0.989$ and the linear equation is shown below:

$$\text{Raman Intensity } (I_{SERS}) = 14515 \text{ Log (TR)} + 67145 \quad (4.4)$$

SY is a synthetic azo dye, which is frequently used in foods due to its low cost was purchased from local market. **Figure 4.11 (a)** shows the characteristic Raman modes of solid SY dye at 986, 1123, 1178, 1231, 1336, 1384, 1496, 1545 and 1594 cm^{-1} and their assignments are given in **Table 4.1**. In the SERS spectrum (**Figure 4.11 (b)**) of SY, the peaks at 1160, 1212, and 1302 cm^{-1} exhibits red shift by 18 cm^{-1}, 19 cm^{-1} and 34 cm^{-1} as compared to solid state Raman spectrum due to N=N stretching, C-C bending and C-N stretching, respectively, which are in good agreement with the literature [18]. These Raman shift demonstrate that $Ag_{0.15}$BOB substrate highly influenced on the SERS spectrum of SY. The detection limit was determined to be 40 µM.

The quantitative analysis of SY was analysed via the selected most intense peak 1593 $cm^{-1}$with an excellent linear response as shown in **Figure 4.11 (c)** in concentration range of 1mM to 40 µM. The linear equation with the correlation coefficient $R^2 = 0.988$ is given below:

$$\text{Raman Intensity } (I_{SERS}) = 2024 \text{ Log (SY)} + 9221 \quad (4.5)$$

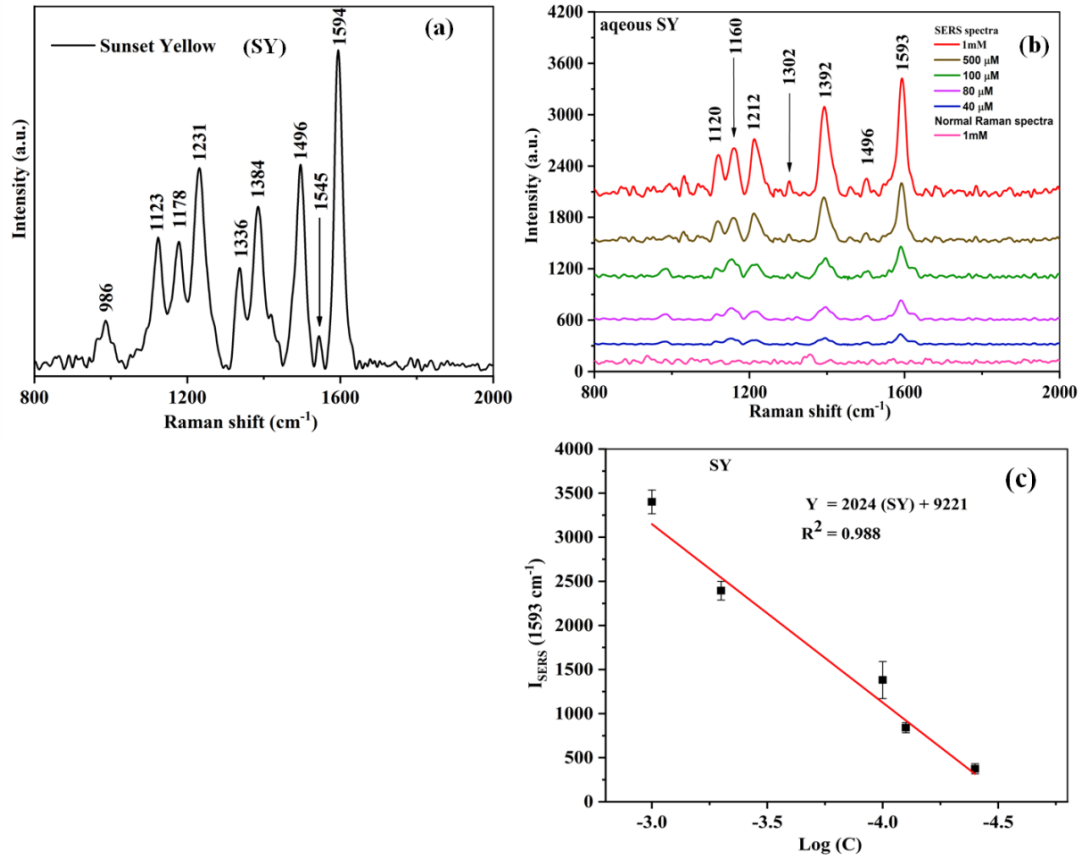

Figure 4.11 *(a) Raman spectra of solid of Sunset yellow (SY) (b) SERS spectra of on* $Ag_{0.15}$ *BOB substrate from 1mM to 40 μM, and calibration plot between the SERS intensity and logarithm concentration of SY.*

The comparison of the detection limits for considered food colorants with the previous report on different SERS substrates are listed in **Table 4.2**.

Substrate	**Analytes**	**LOD (M)**	**Ref**
Bi thin films	R6G	1×10^{-2} M	[40]
Au−BiOI	R6G	0.5×10^{-5} M	[24]
Ag/BR/Ag NPs	TR	2.1×10^{-5} M	[41]
Gold nanodumbells	SY	1.1×10^{-5} M	[42]
$Ag_{0.15}$ BOB	R6G	1.0×10^{-5} M	**This work**
	TR	4.0×10^{-5} M	
	SY	4.0×10^{-5} M	

4.3.8 Analysis of binary mixture of food colors

The SERS analysis of binary mixture with Sunset yellow/ Tartrazine (SY/TR), Sunset yellow SY/AM, Sunset yellow/ Allura red (SY/AR) and Amaranth/Allura red (AM/AR) on $Ag_{0.15}$ BOB offer an examples for the condition that may occur where two food colorants may be present simultaneously.

Figure 4.12 (a-d) demonstrates the SERS spectra using $Ag_{0.15}$ BOB substrate for the detection of binary mixture of food colors, which was prepared by relative ratio of 10^{-3} M concentration of 1:3, 3:1, 1:1, 1:2, 2:1 ratio. The lowest relative ratio at which at least two distinguishable peaks were observed as highlighted in **Figure 4.12** for each colorant. At higher volume ratio with respect to each colors in binary mixture with $Ag_{0.15}$ BOB

substrate, shows the prominent Raman signature of dye, whereas with low relative volume ratio was not detected. Further, we observed that SERS spectra of binary solution of TR with AM and AR were not significantly distinguishable with the used substrate. The SERS spectrum of SY/TR display the characteristic feature of SY at 1302 and 1392 cm^{-1} and TR at 1358, 1214, can be well differentiate these dyes in binary solution. In addition, some of the spectral bands observed, which are closely related to the Raman bands of dyes SY and TR by slight difference, located in the mixture of both colorants as shown in **Figure 4.12 (a)**. **Figure 4.12 (b)** demonstrates the SERS spectra of binary mixture of SY/AM on $Ag_{0.15}$ BOB substrate, the main difference is noticed with the typical 1300, 1590 cm^{-1}signal of SY and 1360, 1474, 1572 cm^{-1} of AM, which are evident in dye mixtures. Similarly, in **Figure 4.12 (c)** SY/AR and in **Figure 4.12 (d)** AM/AR, the predominant spectral features were observed at 1300, 1456 $cm^{-1}$of SY and one peak of AR at 1263 cm^{-1} in SY/AR mixture and the peak at 1363, 1463, 1507 cm^{-1} of AM and the fingerprints at 1340, 1492 cm^{-1} of AR in the mixture of AM/AR can distinguishedthe food colors separately in the binary solution. In addition, some of the spectral bands observed, which appear to be a combination of two bands of SY and TR, SY and AM, SY and AR, AM and AR, located in the mixture of binary colorant solutions and their intensity were also increases as compared to the SERS spectra of individual dye on $Ag_{0.15}$ BOB substrate as shown in **Figure 4.12 (a-d)**. Overall, it was observed that the SERS spectra of dyes show different characteristic bands with different combination of dyes, which may be used as a reference spectral feature for the identification of illegal addition of colours in food stuffs.

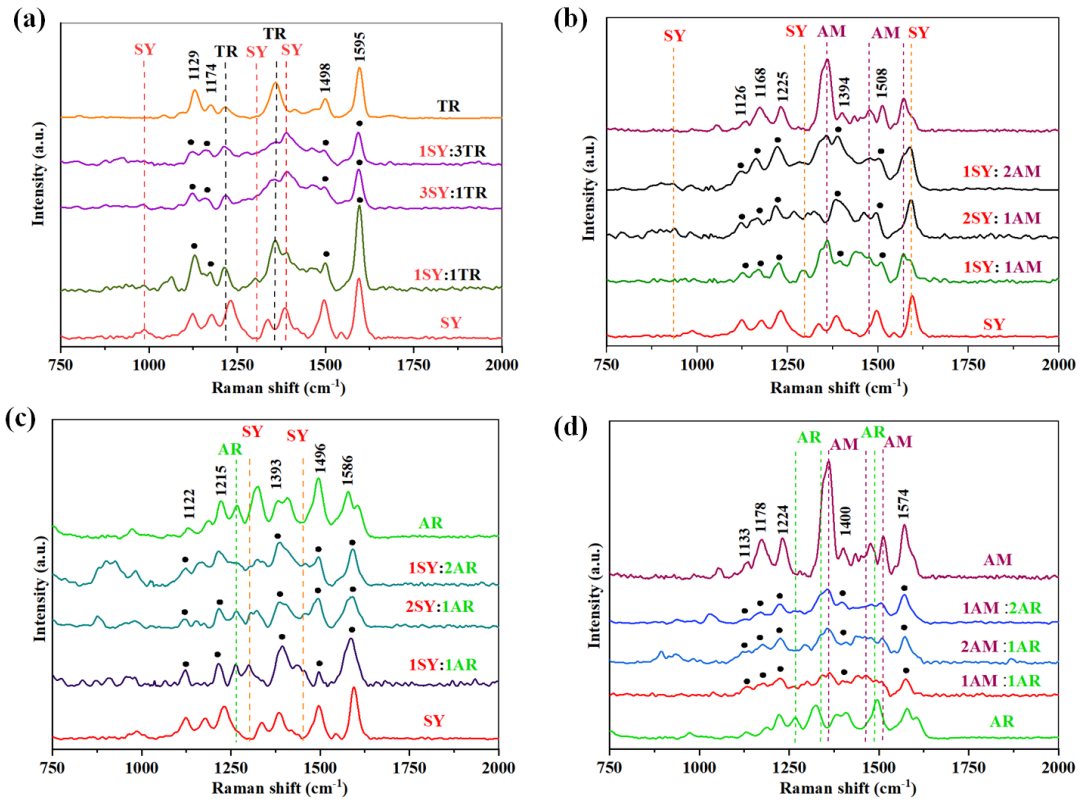

Figure 4.12 *(a) SERS spectra of Tartrazine (TR)/Sunset yellow (SY), (b) Sunset yellow (SY)/Amaranth (AM), (c) Sunset yellow /Allura red (AR), and (d) Allura red/Amaranth at relative ratio 1:3, 3:1, 1:1, 1:2, 2:1 on* $Ag_{0.15}$*BOB substrate.*

Moreover, to validate the stability of the synthesized substrate, 10^{-4} M ethanolic solution of R6G were used as probe molecule, and the SERS spectrum was recorded from eight randomly selected different spots on $Ag_{0.15}$BOB substrate under identical experimental condition. **Figure 4.13 (a)** demonstrates the practically identical SERS spectra with reasonable relative standard deviation (RSD) 9.75% corresponding to the peak at 1507 cm^{-1} as displayed in **Figure 4.13 (b)**. The observed result shows the efficient stability of $Ag_{0.15}$BOB substrate, and makes reliable SERS substrate.

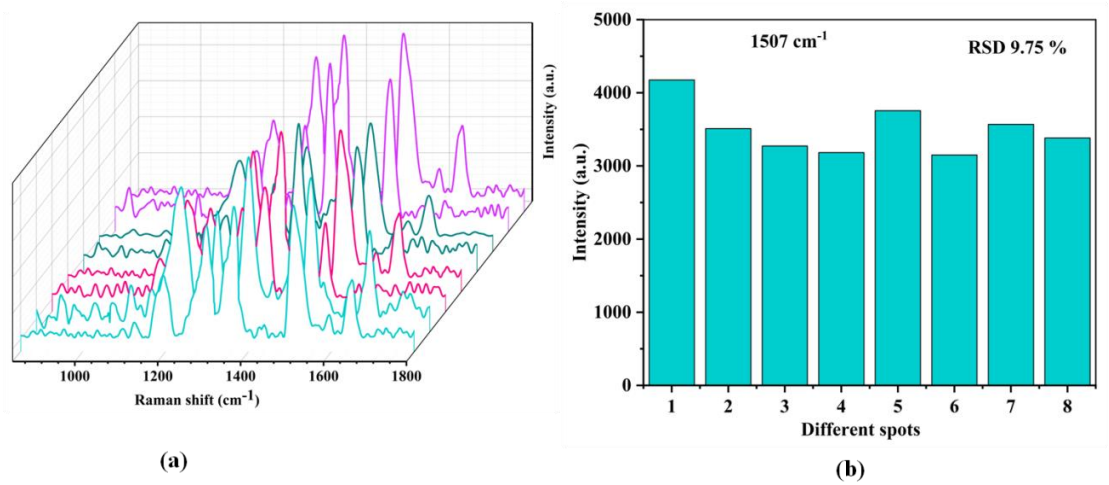

Figure 4.13 *(a) SERS spectra of 10^{-4} M R6G from 8 randomly selected positions (b) Relative standard deviation (RSD) at 1507 cm^{-1}.*

4.4 In situ detection of organic dye Sudan I (SuI) in Chilli powder

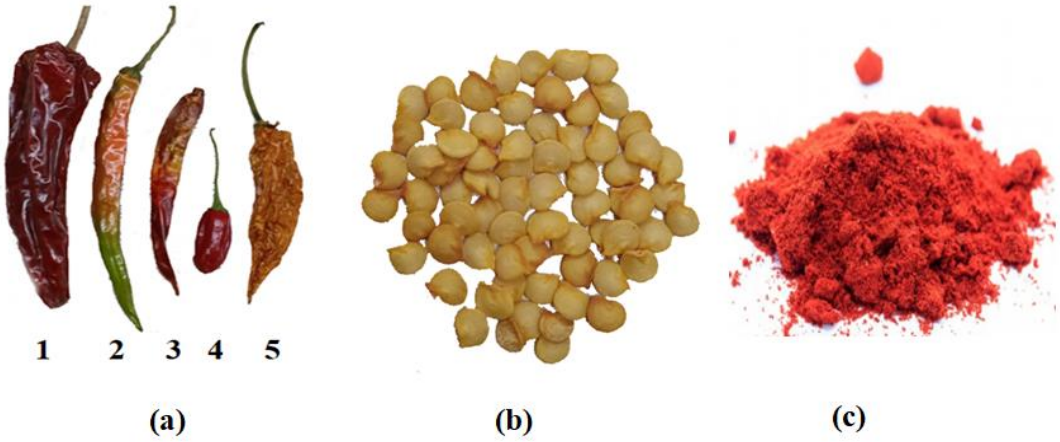

Schematic diagram *of chilli: (a) fruits, (b) seeds, (c) powder.*

The chilli fruits were collected from different varieties. After cleaning the outer layer of fruits with distilled water and acetone, Raman spectrum recorded from the surface of the fruits as well as their seeds were studied for comparison with spectra of chilli powder.

4.4.1 Pretreatment of chilli powder and spiked chilli powder

Three different solvents (acetone, acetonitrile and methanol) with high solubility of Sudan I (SuI) was used to extract unadulterated solution and adulterated SuI from chilli powder. In brief, 100 mg of chilli powder was mixed with 5 ml of the three selected solvents. Then the sample was centrifuged and the brownish red supernatant solution was transferred carefully and used for the analysis of compound present in chilli extract (20, 10, 5, 3, 1, 0.2 mg/mL) as well as for spiking SuI at room temperature. Further, standard known solutions of SuI dye were used to spike the chilli powder, which

gives a series of solution with concentrations: 1mM, 500, 100 and 80 µM. The SERS spectrum was measured for each concentration.

$Bi_{24}O_{31}Br_{10}$ was used as SERS substrate synthesized at 500 ºC following chemical precipitation method as described in Chapter 3, and $Ag_{0.15}$BOB SERS substrate was used in situ detection.

1mg mL^{-1} of extracted solution from unadulterated and 30 µL adulterated samples was mixed with SERS substrates $Bi_{24}O_{31}Br_{10}$, and $Ag_{0.15}$BOB. The sample was dried before being subjected to a SERS test at room temperature after the mixture had been thoroughly mixed and deposited onto the glass slide. Raman and SERS spectra were recorded with integration time 5s and 8s at 80 mW respectively.

4.4.2 Raman analysis of chilli fruits, chilli seeds, and chilli powder

The Raman spectrum of five different varieties of chilli fruits, their seeds and different chilli powder were collected from their surfaces with 785 nm excitation for comparative analysis, which have comparable spectral characteristics but differ in Raman intensity and peak position, and whose vibrational modes are listed in **Table 4.3**. Previous research demonstrates that different red chilli varieties have varied chemical profiles that tend to develop at a dark red color, and this may be because carotenoids are present. Because of the interaction of naturally existing carotenoids with plant species, which is responsible for the changes in their chemical composition or physical structure, the vibrational modes of Raman peaks are influenced [40].

Chilli fruits

Figure 4.14 (a) shows the Raman spectrum of chilli fruits (labeled as number '4') with the peaks at 945, 1003, 1151, 1182, 1517 cm^{-1} which display the characteristic peaks of carotenoids and their assignments are in **Table 4.2**. In another chilli fruits labeled as '1, 2(red part), 3 and 5' in **Figure 4.14 (a)**, the observed peak at 945 cm^{-1} was not appeared and there is a variation in the intensity of the appeared peaks, which arises due to the different content of carotenoids [41-42]. These observed peaks at 945, 1182 can be allocated to C-H symmetric and wagging of CH_3 group, and in phase C–C stretching vibrations of the main polyene chain, respectively. The peaks at 1003, 1151 and 1517 cm^{-1} corresponds to C-CH_3 in plane group rocking mode, C-C, and C=C stretching bond, designated as v_3, v_2 and v_1, respectively. Appearance of these Raman modes demonstrates the presence of carotenoids as major constituents in chilli fruit [40, 42-43]. The major peaks of the red chilli fruit are observed at 1517, 1151, 1182 and 1003 cm^{-1} corresponds to the capsanthin, the main carotenoid in red chilli during ripening [44-45].

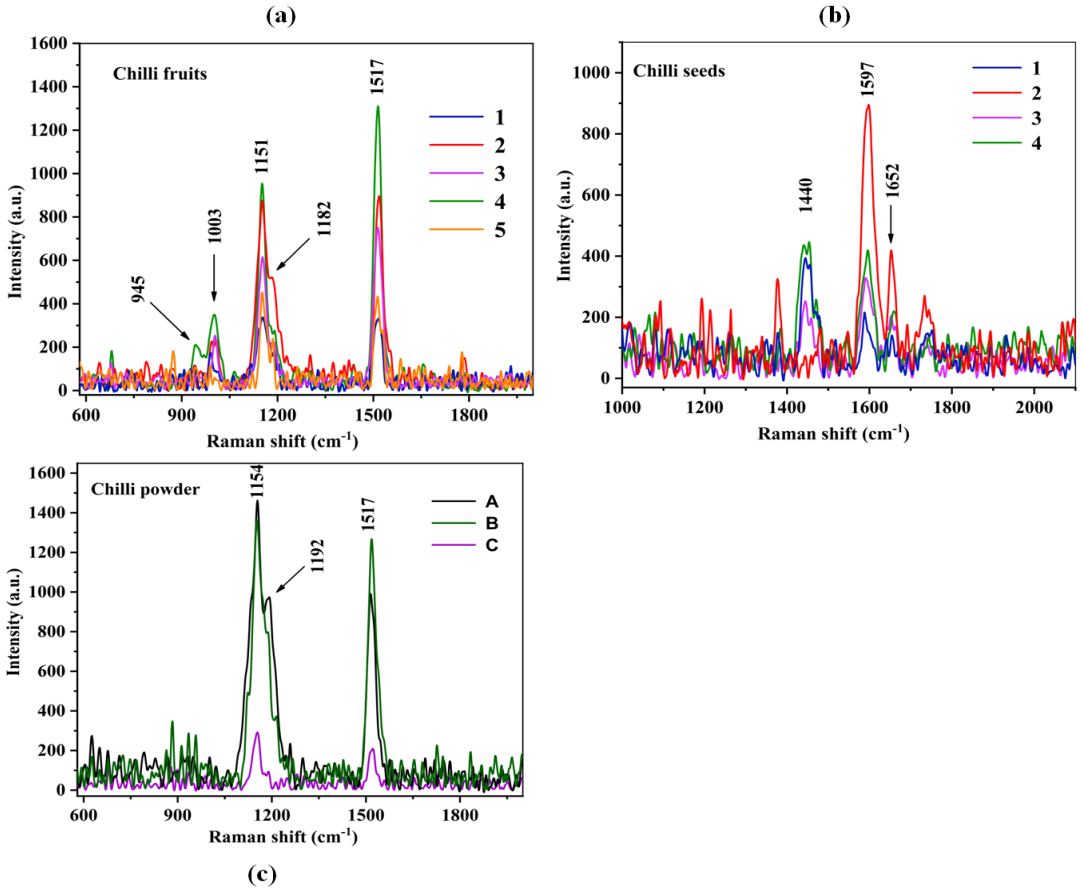

Figure 4.14 *Raman spectrum of different chilli samples (a) chilli fruits and (b) chilli seeds, and (c) chilli powder.*

Chilli seeds

The Raman spectra of the selected chilli fruit seeds are shown in **Figure 4.14 (b)**. These seeds have different spectral features than chilli fruits, demonstrating the presence of several chemicals. Three primary peaks were found at 1440, 1597, and 1652 cm^{-1}, and different kinds of the seeds under consideration showed a shift in peak position and variation in the intensity. The most intense peak at 1597 cm^{-1} attributed to nicotinic acid and another peak at 1652 cm^{-1} can be assigned to C=C stretching bond. The peak at

1440 cm^{-1} arises due to the C-H in plane bending. The observed peaks at 1650 and 1440 cm^{-1} may be due to fatty acid as palmitic acid [46].

Chilli powder

Figure 4.14 (c) shows the Raman spectrum of chilli powder. Three significant peaks were found in the Raman spectrum of chilli powder, located at 1154, 1192 and 1517 $cm^{-1}$and these peaks exhibit nearly identical spectral characteristics with slight variations in Raman intensity and peak position when compared to chilli fruits. The sharp peaks were appeared at 1517 and 1154 cm^{-1} in the red chilli powder can be assigned to v_2 and v_1 Raman modes and the shoulder at 1192 cm^{-1} of shows red shift by 10 cm^{-1} than fruit in chilli powder, which represent the characteristic fingerprints of carotenoids [43].

4.4.3 SERS studies of Sudan I dye

To compare the results and chemical species, we further analysed the SERS spectrum using $Bi_{24}O_{31}Br_{10}$ and $Ag_{0.15}$BOB substrate and **Figure 4.15 (a)** represents the SERS spectrum of chilli extract on $Bi_{24}O_{31}Br_{10}$ and $Ag_{0.15}$BOB substrate. The enhancement in Raman signal demonstrates that $Bi_{24}O_{31}Br_{10}$ can act as good SERS substrate as compared to $Ag_{0.15}$BOB. Further, $Bi_{24}O_{31}Br_{10}$substrate was used for the detection of chilli extract in three different solvents with the characteristic peaks of carotenoids appeared at 951, 1000, 1152, 1189, 1257, 1436 and 1519 cm^{-1}as illustrated in Figure 4.15 (b). The shoulder peak shown in the spectrum peaks at 1263 and 1434 cm^{-1} corresponds to β-carotenoid and $\delta(CH_2)$ mode of Cuticular wax carotene, respectively [47]. The major peaks observed in the SERS spectrum are consistent with the Raman

spectrum of chilli powder and fruits. Thus, the observed results demonstrate that chemical composition in chilli fruits, seeds and powder can be distinguished and identified by using Raman and SERS spectroscopy. The detection of adulterants in chilli products can be complicated by these chemical species, as would be covered in more depth below.

Effect of solvent

In order to extract SuI with the greatest solubility and extraction efficiency possible and to prevent the in-situ solubility of contaminants from chilli powder, an appropriate solvent with a high solubility of SuI in chilli powder was selected. Despite their great solubility, acetonitrile, acetone, and methanol might have different affinities for other chemicals due to changes in their polarity and the dimensions of molecules [48-49]. As a result, Raman and SERS spectra were conducted to compare their affinities towards compounds in chilli powder, and the spectral features are displayed in **Figure 4.14 (c)** and **Figure 4.15 (a)**. Raman spectrum of chilli powder in different solvents recorded in the range of 900-2000 cm^{-1} as shown in **Figure 4.15 (b)** were compared with 1mg mL^{-1} of same chilli brand. In comparison to acetone and methanol, acetonitrile has great solubility, has a higher affinity for the chemical in chilli powder, and displays prominent peaks within the target region. Acetonitrile was applied as a solvent for further examination of the samples' Raman spectra.

Three distinct brands of chilli powder samples in acetonitrile at various concentrations (20, 10, 5, 3, 1, 0.2 mg mL^{-1}) were examined using SERS substrate to determine the differences between the various brands. **Figure 4.15 (b)** shows the linear regression model plotted between concentration and intensity of three different chilli extract and

resulted in the R^2 values of 0.9934, 0.9836, 0.9709, respectively for selected vibrational band at 1519 cm^{-1}. The high value of R^2 demonstrates the good linear correlation between them and the variation in intensity may be due to different content of carotenoids present in three different brands of chilli.

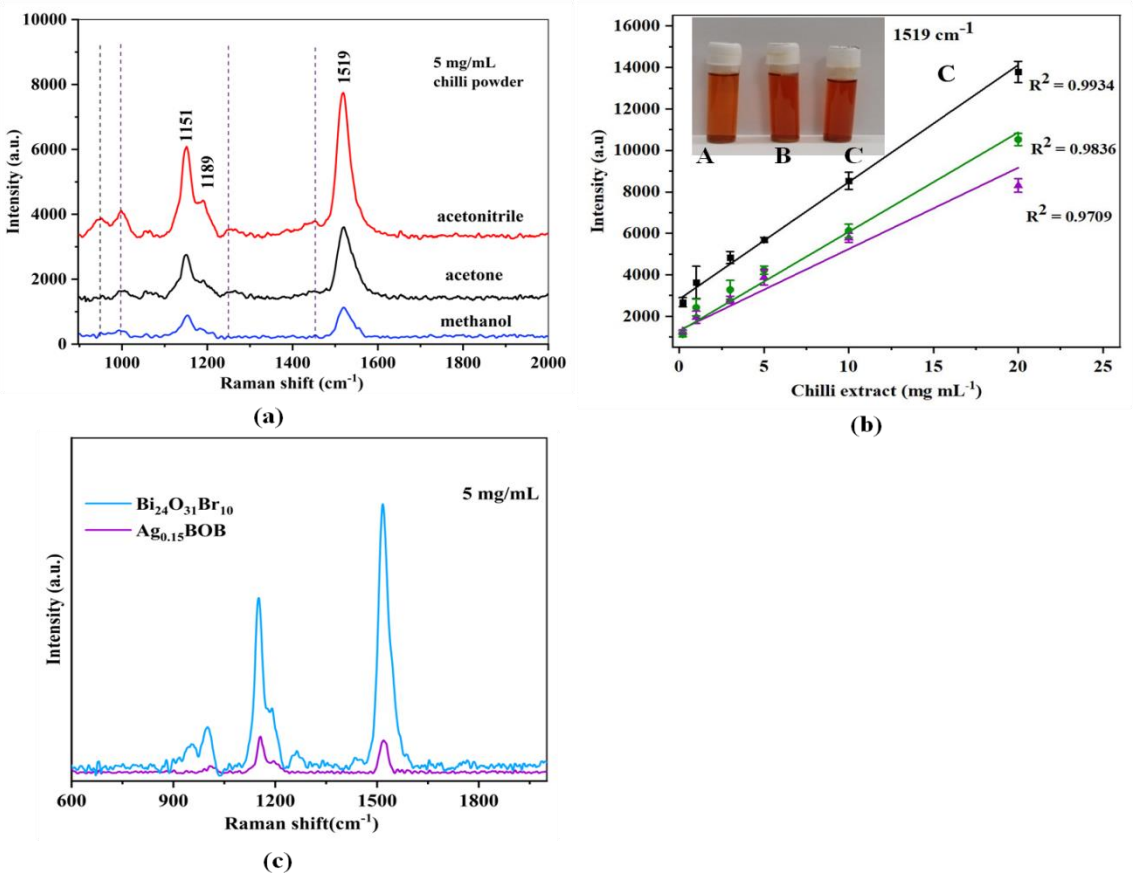

Figure 4.15 *SERS spectrum of chilli extract on $Bi_{24}O_{31}Br_{10}$ (a) in different solvents (b) in acetonitrile for three different brands.*

The Raman spectrum of solid SuI is depicted in **Figure 4.16 (a)**, and Table 4.1 includes the main characteristic peaks' assignments as follows at 986, 1094, 1169, 1226, 1337, 1387, 1494, 1547, and 1593 cm^{-1} and their assignment are given in **Table**

4.1. Further, Raman spectra of 10 mM SuI in acetonitrile and SERS spectrum of Sudan I were recorded to compare enhancement in SERS signals as shown in **Figure 4.16 (b)**. $Bi_{24}O_{31}Br_{10}$ was selected as a SERS substrate for the detection of a series of standard solutions Sudan I from 1mM to 80 μM. The observed SERS peaks are well consistent with the Raman spectrum of pure solid SuI dye. In the SERS spectrum, the sharp peak at 1592 cm^{-1} corresponds to the stretching of C-C bond, C-H in plane deformation and other prominent peaks at 1382 and 1221 cm^{-1} can be assigned to C-N, C-C stretching in benzene ring and C-H in plane bending of phenyl groups, respectively. The obtained results are well matched with the previous results [50]. The lowest detection limit for SuI was determined to be 80 μM, which was closer to the detection limit with 100 μM on gold colloids reported by Cheung et al [13].

The calibration plot of SuI display (**Figure 4.16 (c)**) that as concentration decreases from 1mM to 80 μM the intensity of the Raman peak at 1592 cm^{-1} decreases. The correlation coefficient $R^2 = 0.984$ with the linear equation as follows:

$$\text{Raman Intensity } (I_{SERS}) = 2387 \text{ Log (SuI)} + 10467 \quad (4.6)$$

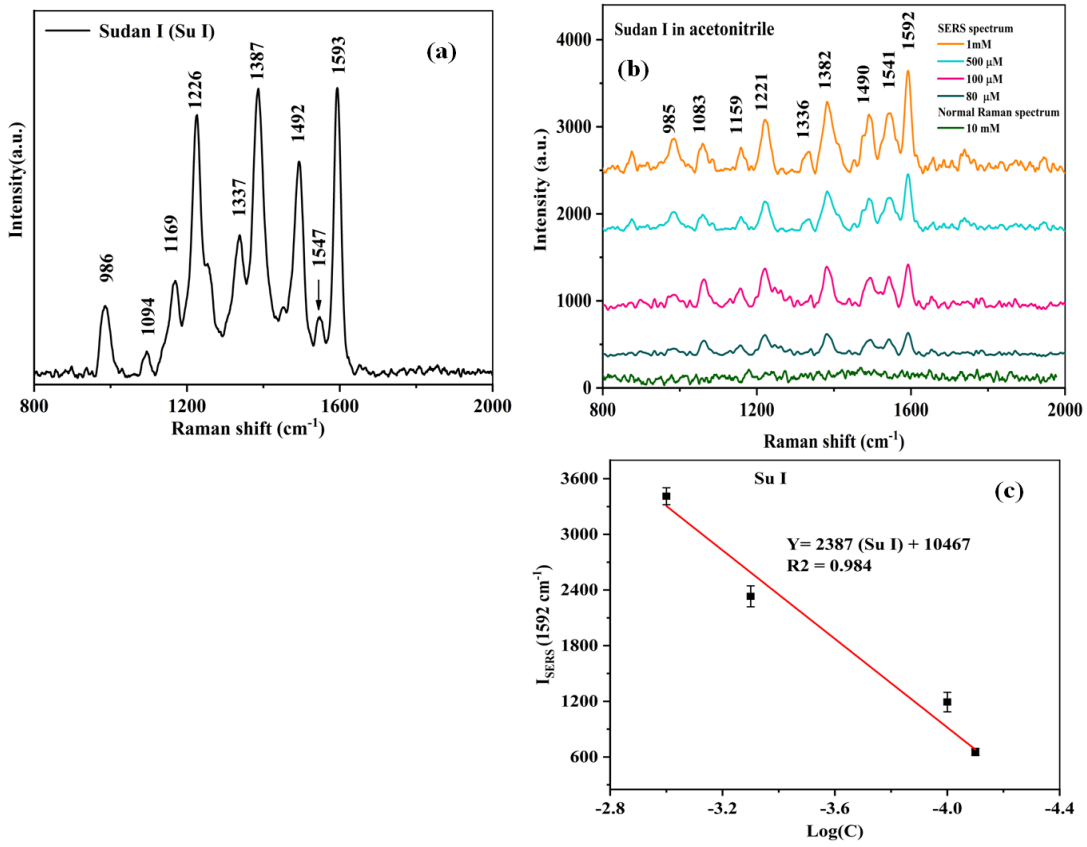

Figure 4.16 *(a) Raman spectra of Sudan I (SuI) (b) SERS spectra of Sudan I on* $Bi_{24}O_{31}Br_{10}$ *from 1mM to 80 µM (c) calibration plot between intensity and logarithmic concentration of SuI.*

4.4.4 Detection of spiked Sudan I in chilli powder

Figure 4.17 represents the SERS spectrum of spiked SuI (500 µM) in chilli extract and compared to the SERS spectrum of without spiked chilli extract (1mg mL^{-1}) as well as the SERS spectrum of the standard solution of 1mM SuI in acetonitrile. The SERS spectrum of chilli extract (**Figure 4.17 (a)**) shows two major peaks at 1516, 1152 cm^{-1} and a shoulder peak at 1000 cm^{-1} arises due to the carotenoide in chilli extract. However, in the spiked SERS spectrum, the additional peaks of the other chilli components were

not seen (in **Figure 4.17 (b)**) because of these three peaks were overlapped with the SuI. The major peaks of Sudan at 1490, 1159 and 985 cm^{-1} is shown in **Figure 4.17 (c)**. In addition, the SERS intensity of the characteristic peaks of SuI was higher at 1mM as compared to SERS intensity of spiked SuI and the relative intensity of the compound present in chilli extract was low. While, the peak intensity of chemicals in chilli extract were higher and interfere with the peaks of spiked species SuI at lower concentration adsorbed on $Bi_{24}O_{31}Br_{10}$ substrate. The reason behind the weak intensity of spiked species may be due to the fluorescence of compound in chilli extract which can suppressed the characteristic peaks of SuI as shown in **Figure 4.17 (d)** at 80 μM concentration, and **Figure 4.17 (d)** represents the SERS spectrum of spiked SuI from 1mM to 80 μM on $Bi_{24}O_{31}Br_{10}$ substrate. Thus, the results show that with the increased sensitivity of SERS substrate at lower concentration, we can distinguish compound in chilli powder and illegally added dyes in chilli.

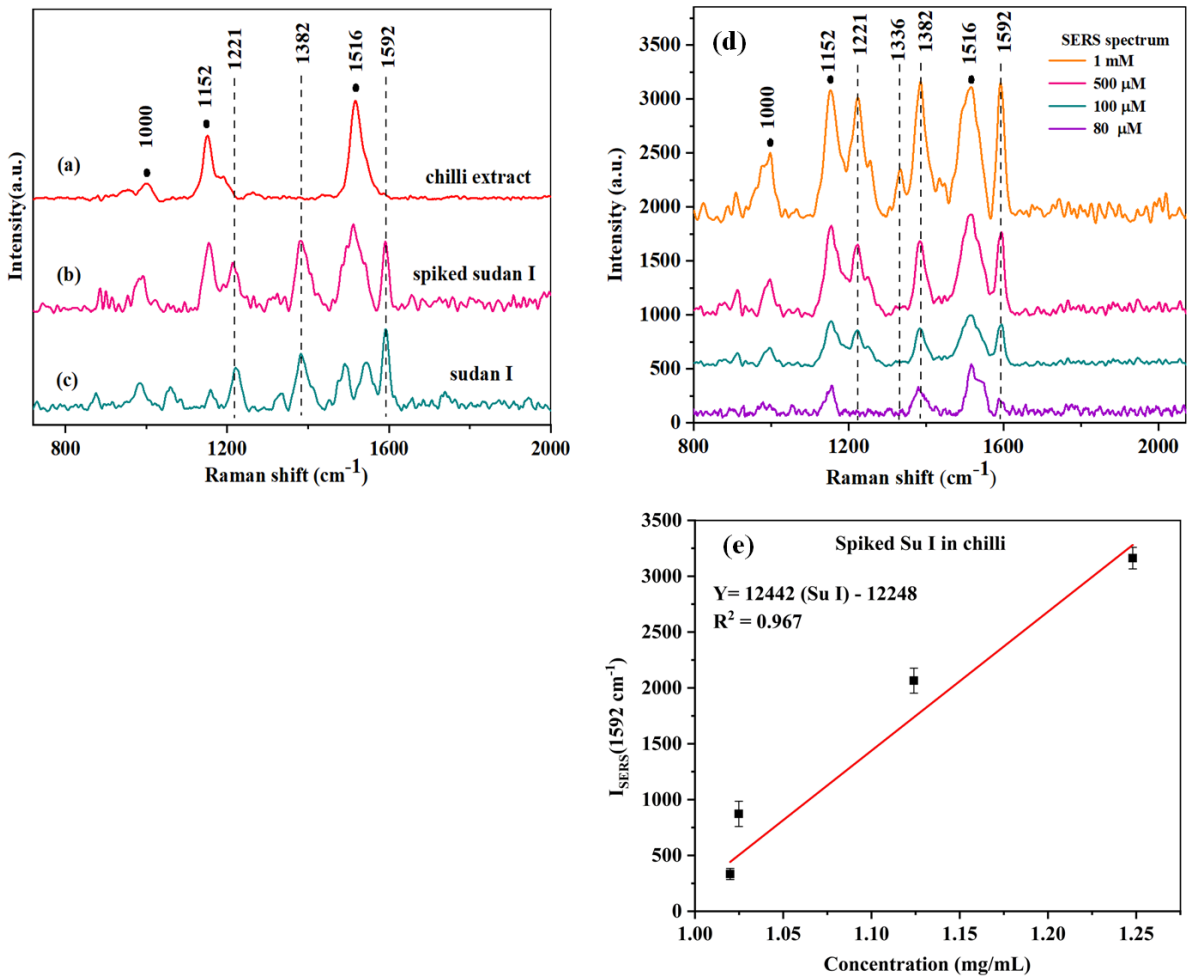

Figure 4.17 *SERS spectra of (a) chilli extract (1mg mL^{-1}) (b) spiked SuI (500 µM) in chilli extract (1mg mL^{-1}) (c) 1mM SuI (d) spiked sudan I (into chilli extract 1 mg mL^{-1}) from 1mM to 80 µM (e) the relation between Raman intensity at the peak 1592 cm^{-1}and concentration of spike SuI in chilli powder.*

The recovery was evaluated by spiking SuI with known concentration of chilli powder at three levels 10.9×10^{-2}, 5.5×10^{-2}, 2.5×10^{-2} mg mL^{-1} in order to verify the validity and applicability of this detection approach as shown in **Table 4.4**. On the basis of measured intensity corresponding to most prominent peak at 1592 cm^{-1} in the Raman spectra, the concentration of SuI were calculated. Recovery of this method for detecting

SuI in chilli powder between 97.9 to 99.8 %, which indicate the reliable and accurate recovery SuI in chilli powder.

Table 4.4 Recovery of Sudan I concentrations in chilli powder

Extract concentration (mg mL^{-1})	**Spiked concentration (mg mL^{-1})**	**Calculated concentration (mg mL^{-1})**	**Recovery (%)**
1.0 mg/mL	0	1.0	100
	10.9×10^{-2}	1.086	97.9
	5.5×10^{-2}	1.048	99.3
	2.5×10^{-2}	1.023	99.8

4.5 Conclusion

In summary, the CTAB assisted-BiOBr and CTAB-AgBr- Bi_3O_4Br/BiOBr microparticles with different amount of silver via chemical precipitation method was successfully synthesized. Further it was demonstrated that these microparticles such as BOB, $Ag_{.09}$BOB, and $Ag_{0.15}$BOB can be used as SERS substrates with high sensitive detection. The composites with $Ag_{0.15}$BOB exhibits excellent SERS activity in comparison to other substrates. The SERS activity was verified by the detection of R6G in ethanol and the lowest detection limit was found to be 10 μM. The above microparticles were also allowed for the detection of food colorants in aqueous solution as AR, AM, TR and SY. The limit of detection was determined to be 50 μM for AR, AM and 40 μM for TR and SY.

Further, SERS activity of novel substrates Bismuth oxybromide ($Bi_{24}O_{31}Br_{10}$), and $Ag_{0.15}$BOBwere analysed by the detection of real samples. Raman spectroscopy with 785 nm was performed for the direct detection of chemical species in chilli fruits, seeds, and powders as well as illegal addition of dye SuI. The vibrational modes of chilli species reveals different compounds are present in different species. Moreover, SERS study of chilli extract demonstrates that $Bi_{24}O_{31}Br_{10}$ SERS substrate has significant spectral feature compare to $Ag_{0.15}$BOB substrate after the adsorption of extract. These features can identify the chemical compound present in chilli powder accurately and SERS spectra of SuI in acetonitrile were collected with the detection of unadulterated and adulterated chilli powder. The detection limit of chilli extract was found to be 0.2 mg mL^{-1} and for spiked SuI was determined to be 100 μM on $Ag_{0.15}$BOB, and80 μM on $Bi_{24}O_{31}Br_{10}$. Thus Bismuth based material can be utilized as a SERS substrate for the detection of compound in chilli species and adulterated SuI and can play role for the investigation of impurities in food fraud in future. Thus the developed method can act as a promising tool over conventionally used methods for rapid quantitative detection of adulteration of colorants in chilli or other food fraud in future in a label-free and non-invasive manner.

Table 4.1 Tentative assignment of Rhodamin 6G, Allura red, Amaranth, Tartrazine, and Sunset yellow

Analytes	**Raman shift (cm^{-1})**	**Tentative assignment**
Rhodamin 6G	607	ipδ(C-C-C) ring
	768	op δ(C-H)
	1117/1179	ip δ(C-H)
	1302	ipδ(N-H)
	1360/1504/1593/1644	ν (C-C) Ref [35], [36]
Allura red	751	$\omega(R_1)$
	974	ω(C-H)R_2
	1129/1578	$\nu_{as}(R_1)$
	1188	$\nu_{as}(SO_2)$
	1223	ρ (C-H- R_1)
	1266	ν(O-C- R_1)
	1383/1496	ω(C-H)
	1407	ρ (C-H)
	1604	ν_{as} (R_2) Ref [17]
Amaranth	738	ρ(C-H)
	1052	ν_{as} (SO_2)
	1138/1175	ω(C-H)
	1231	ω(O-S)
	1363	ν(C-C)
	1405/1434	ω(C-H)
	1478	ν (N-N)
	1572	ν_{as} (ring) Ref [37] [38]
Tartrazine	623	def(R1)
	802	ν(C-O)
	1044	op (C – H); def. (R2)
	1132	op def(C-H-R1); δ(R1)

	1177	τ(R1)
	1217	ν(R1)
	1361	ν(C-N=N-C); νs(COO); wagg(R1)
	1414	ν(R1)
	1499	δ(R1); δ(C=C)
	1597	δ(R1);ip def(C-H-R1); δ(O-H); νs(COO)
		Ref [39]
Sunset yellow	986	ω(C-H-R_2)
	1123	ν (N=N); ω(C-H- R_1)
	1178	ν (N=N); ρ(C-H-R_1); ρ(R_1)
	1231	δ(C-C-R_1); ν (C-N); ν (C-C- R_2);
	1336	ν (C-N); ν_{as}(H-C-C-H-R_1); ρ(R_1)
	1384	ν_s(C-C-R_2); ip δ(R_1, R_2)
	1496	ν (C-N); ν (C-O); ρ(N-H)
	1545	δ(C-C-R_2); ρ(N-H); ρ(C-H)
	1594	ν_s(C-C-R_1); ω(C-H-R_1)
		Ref [18]

Table 4.3 Tentative assignment of Raman modes of chilli and Sudan I

Samples	**Raman shift (cm^{-1})**	**Assignment**
Chilli (fruits, powder)	945-951	ν_s (C-H), ω(CH_3)
	100-1003	ρ_{ip} (C-CH_3)
	1154	ν_s (C-C)
	1182-1192	ip (C–C)
	1263	δ_{ip}(=C-H)
	1434	δ(CH_2)
	1517	ν_s (C=C)
		Ref [40] [47] [43]

Sudan I	986	δCCC
	1094	ipCCC, δCH, ν_sC=N
	1169	δCH
	1226	ν_sCC, δCH, ν_sC–NH
	1337	ν_sCC, δCH
	1387	ν_sC═N, δNH, ν_sCC,
	1492	δCH ν_sCC, δCH, ν_sC–NH
	1547	δNH, γ_sC═N, ν_sC═O
	1593	ν_sCC, δCH, δNH
		Ref [49]

(δ = deformation ((bending/scissoring)), ω = wagging, ip = in plane, ρ = rocking, ν_s = symmetric stretching)

References:

[1] N. Martins, C. L. Roriz, P. Morales, L. Barros, and I. C. F. R. Ferreira, "Food colorants: Challenges, opportunities and current desires of agro-industries to ensure consumer expectations and regulatory practices," *Trends food Sci. Technol.*, vol. 52, pp. 1–15, 2016.

[2] M. Shahid, Shahid-Ul-Islam, and F. Mohammad, "Recent advancements in natural dye applications: A review," *J. Clean. Prod.*, vol. 53, pp. 310–331, 2013, doi: 10.1016/j.jclepro.2013.03.031.

[3] A. Downham and P. Collins, "Colouring our foods in the last and next millennium," *Int. J. food Sci. Technol.*, vol. 35, no. 1, pp. 5–22, 2000.

[4] M. Carocho, M. F. Barreiro, P. Morales, and I. C. F. R. Ferreira, "Adding molecules to food, pros and cons: A review on synthetic and natural food additives," *Compr. Rev. food Sci. food Saf.*, vol. 13, no. 4, pp. 377–399, 2014.

[5] D. McCann *et al.*, "Food additives and hyperactive behaviour in 3-year-old and 8/9-year-old children in the community: a randomised, double-blinded, placebo-controlled trial," *Lancet*, vol. 370, no. 9598, pp. 1560–1567, 2007, doi: https://doi.org/10.1016/S0140-6736(07)61306-3.

[6] R. E. Wrolstad and C. A. Culver, "Alternatives to those artificial FD&C food colorants," *Annu. Rev. Food Sci. Technol.*, vol. 3, pp. 59–77, 2012.

[7] H. Rahnama, S. M. Mazloomi, E. Berizi, A. Abbasi, and Z. Gholami, "Identification of Tartrazine adulteration and evaluating exposure to synthetic dyes of sunset yellow and Quinoline yellow through consumption of food products among children," *Food Sci. Nutr.*, vol. 10, no. 11, pp. 3781–3788, 2022.

[8] K. Rovina, S. Siddiquee, and S. M. Shaarani, "Extraction, analytical and advanced methods for detection of allura red AC (E129) in food and beverages products," *Front. Microbiol.*, vol. 7, p. 798, 2016.

[9] S. He *et al.*, "Multivariate qualitative analysis of banned additives in food safety using surface enhanced Raman scattering spectroscopy," *Spectrochim. Acta Part A Mol. Biomol. Spectrosc.*, vol. 137, pp. 1092–1099, 2015.

[10] S. Dixit, S. K. Purshottam, S. K. Gupta, S. K. Khanna, and M. Das, "Usage pattern and exposure assessment of food colours in different age groups of consumers in the State of Uttar Pradesh, India," *Food Addit. Contam.*, vol. 27, no. 2, pp. 181–

189, 2010.

[11] D. Benford *et al.*, "Application of the Margin of Exposure (MOE) approach to substances in food that are genotoxic and carcinogenic," *Food Chem. Toxicol.*, vol. 48, pp. S2–S24, 2010.

[12] J. C. Moore, J. Spink, and M. Lipp, "Development and application of a database of food ingredient fraud and economically motivated adulteration from 1980 to 2010," *J. Food Sci.*, vol. 77, no. 4, pp. R118–R126, 2012.

[13] W. Cheung, I. T. Shadi, Y. Xu, and R. Goodacre, "Quantitative analysis of the banned food dye Sudan-1 using surface enhanced Raman scattering with multivariate chemometrics," *J. Phys. Chem. C*, vol. 114, no. 16, pp. 7285–7290, 2010.

[14] W. Chai, H. Wang, Y. Zhang, and G. Ding, "Preparation of polydopamine-coated magnetic nanoparticles for dispersive solid-phase extraction of water-soluble synthetic colorants in beverage samples with HPLC analysis," *Talanta*, vol. 149, pp. 13–20, 2016.

[15] F. Soponar, A. C. Moţ, and C. Sârbu, "Quantitative determination of some food dyes using digital processing of images obtained by thin-layer chromatography," *J. Chromatogr. A*, vol. 1188, no. 2, pp. 295–300, 2008.

[16] M. Ma, X. Luo, B. Chen, S. Su, and S. Yao, "Simultaneous determination of water-soluble and fat-soluble synthetic colorants in foodstuff by high-performance liquid chromatography–diode array detection–electrospray mass spectrometry," *J. Chromatogr. A*, vol. 1103, no. 1, pp. 170–176, 2006.

[17] Y. Yao *et al.*, "Highly reproducible and sensitive silver nanorod array for the rapid detection of Allura Red in candy," *Spectrochim. Acta Part A Mol. Biomol. Spectrosc.*, vol. 195, pp. 165–171, 2018.

[18] Y. Xie, T. Chen, Y. Cheng, H. Wang, H. Qian, and W. Yao, "SiO2@ Au nanoshells-based SERS method for detection of sunset yellow and chrysoidine," *Spectrochim. Acta Part A Mol. Biomol. Spectrosc.*, vol. 132, pp. 355–360, 2014.

[19] K. Kneipp *et al.*, "Surface-enhanced Raman spectroscopy in single living cells using gold nanoparticles," *Appl. Spectrosc.*, vol. 56, no. 2, pp. 150–154, 2002.

[20] P. J. Arathi, S. Bhaskar, G. Rajendra Kumar Reddy, P. Suresh Kumar, and V. Ramanathan, "The photocatalytic role of electrodeposited copper on pencil graphite," *Phys. Chem. Chem. Phys.*, vol. 20, no. 5, pp. 3430–3432, 2018, doi:

10.1039/c7cp08383a.

[21] A. M. Ganose, M. Cuff, K. T. Butler, A. Walsh, and D. O. Scanlon, "Interplay of orbital and relativistic effects in bismuth oxyhalides: BiOF, BiOCl, BiOBr, and BiOI," *Chem. Mater.*, vol. 28, no. 7, pp. 1980–1984, 2016.

[22] V. Q. Nguyen, M. A. Mahadadalkar, A. M. Rabie, and J. J. Shim, "Microwave-assisted synthesis of a Z-scheme heterojunction Ag/AgBr@ BiOBr/Bi2O3 photocatalyst for efficient organic pollutant degradation under visible light," *Environ. Sci. Nano*, vol. 9, pp. 1724–1737, 2022.

[23] L. Kong *et al.*, "Unusual reactivity of visible-light-responsive AgBr–BiOBr heterojunction photocatalysts," *J. Catal.*, vol. 293, pp. 116–125, 2012.

[24] M. D. Prasad, M. G. Krishna, and S. K. Batabyal, "Facet-Engineered Surfaces of Two-Dimensional Layered BiOI and Au–BiOI Substrates for Tuning the Surface-Enhanced Raman Scattering and Visible Light Photodetector Response," *ACS Appl. Nano Mater.*, vol. 2, no. 6, pp. 3906–3915, Jun. 2019, doi: 10.1021/acsanm.9b00771.

[25] M. Muniz-Miranda, "SERS monitoring of the catalytic reduction of 4-nitrophenol on Ag-doped titania nanoparticles," *Appl. Catal. B Environ.*, vol. 146, pp. 147–150, 2014, doi: 10.1016/j.apcatb.2013.03.008.

[26] C. H. Sun, M. L. Wang, Q. Feng, W. Liu, and C. X. Xu, "Surface-enhanced Raman scattering (SERS) study on Rhodamine B adsorbed on different substrates," *Russ. J. Phys. Chem. A*, vol. 89, no. 2, pp. 291–296, 2015, doi: 10.1134/S0036024415020338.

[27] B. D. Cullity, *Elements of X-ray Diffraction*. Addison-Wesley Publishing, 1956.

[28] B. Han *et al.*, "Improved charge transfer contribution by cosputtering Ag and ZnO," *Nanomaterials*, vol. 10, no. 8, p. 1455, 2020.

[29] P. Xu, J. Yang, Y. Chen, Y. Li, X. Jia, and H. Song, "Wood-derived fiber/BiOBr/AgBr sponges by in situ synthesis for separation of emulsions and degradation of dyes," *Mater. Des.*, vol. 183, p. 108179, 2019.

[30] P. Singh *et al.*, "Enhanced photocatalytic activity and stability of AgBr/BiOBr/graphene heterojunction for phenol degradation under visible light," *J. Saudi Chem. Soc.*, vol. 23, no. 5, pp. 586–599, 2019.

[31] G. Su, C. Yang, and J.-J. Zhu, "Fabrication of gold nanorods with tunable longitudinal surface plasmon resonance peaks by reductive dopamine," *Langmuir*,

vol. 31, no. 2, pp. 817–823, 2015.

[32] J. Tang, J. Huang, and S.-Q. Man, "Preparation of gold nanoparticles by surfactant-promoted reductive reaction without extra reducing agent," *Spectrochim. Acta Part A Mol. Biomol. Spectrosc.*, vol. 103, pp. 349–355, 2013.

[33] Z. M. Sui *et al.*, "Capping effect of CTAB on positively charged Ag nanoparticles," *Phys. E Low-dimensional Syst. nanostructures*, vol. 33, no. 2, pp. 308–314, 2006.

[34] A. L. Dendramis, E. W. Schwinn, and R. P. Sperline, "A surface-enhanced Raman scattering study of CTAB adsorption on copper," *Surf. Sci.*, vol. 134, no. 3, pp. 675–688, 1983.

[35] L. Jensen and G. C. Schatz, "Resonance Raman scattering of rhodamine 6G as calculated using time-dependent density functional theory," *J. Phys. Chem. A*, vol. 110, no. 18, pp. 5973–5977, 2006.

[36] X. N. He *et al.*, "Surface-enhanced Raman spectroscopy using gold-coated horizontally aligned carbon nanotubes," *Nanotechnology*, vol. 23, no. 20, p. 205702, 2012.

[37] Q. Zou, Y. Yao, W. Wang, J. Li, C. Yan, and C. Han, "Study on detection of pigment Amaranth based on surface-enhanced Raman scattering," in *2018 Cross Strait Quad-Regional Radio Science and Wireless Technology Conference (CSQRWC)*, 2018, pp. 1–3.

[38] N. Peica, I. Pavel, S. Cîntă Pînzaru, V. K. Rastogi, and W. Kiefer, "Vibrational characterization of E102 food additive by Raman and surface-enhanced Raman spectroscopy and theoretical studies," *J. Raman Spectrosc. An Int. J. Orig. Work all Asp. Raman Spectrosc. Incl. High. Order Process. also Brillouin Rayleigh Scatt.*, vol. 36, no. 6-7, pp. 657–666, 2005.

[39] Y. Ai *et al.*, "Rapid qualitative and quantitative determination of food colorants by both Raman spectra and Surface-enhanced Raman Scattering (SERS)," *Food Chem.*, vol. 241, pp. 427–433, 2018.

[40] V. E. de Oliveira, H. V Castro, H. G. M. Edwards, and L. F. C. de Oliveira, "Carotenes and carotenoids in natural biological samples: a Raman spectroscopic analysis," *J. Raman Spectrosc.*, vol. 41, no. 6, pp. 642–650, 2010.

[41] S. Kolasinac, I. Pecinar, D. Danojevic, and Z. D. Stevanovic, "Raman spectroscopy coupled with chemometric modeling approaches for authentication of different paprika varieties at physiological maturity," *LWT-FOOD Sci. Technol.*, vol. 162, 2022.

[42] S. Sharma, A. Sarika Bharti, R. Singh, and K. N. Uttam, "Non-destructive phenotyping of chili pepper ripening using spectroscopic probes: A potential approach for shelf-life measurement," *Anal. Lett.*, vol. 52, no. 10, pp. 1590–1613, 2019.

[43] R. Withnall, B. Z. Chowdhry, J. Silver, H. G. M. Edwards, and L. F. C. de Oliveira, "Raman spectra of carotenoids in natural products," *Spectrochim. acta part a Mol. Biomol. Spectrosc.*, vol. 59, no. 10, pp. 2207–2212, 2003.

[44] H. Schulz, M. Baranska, and R. Baranski, "Potential of NIR-FT-Raman spectroscopy in natural carotenoid analysis," *Biopolym. Orig. Res. Biomol.*, vol. 77, no. 4, pp. 212–221, 2005.

[45] R. Baranski, M. Baranska, and H. Schulz, "Changes in carotenoid content and distribution in living plant tissue can be observed and mapped in situ using NIR-FT-Raman spectroscopy," *Planta*, vol. 222, pp. 448–457, 2005.

[46] A. G. Barua, S. Hazarika, J. S. Pathak, and C. Kalita, "Spectroscopic investigation of the seeds of chilli (Capsicum annum L.)," *Int. J. Food Sci. Nutr.*, vol. 59, no. 7–8, pp. 671–678, 2008.

[47] J. Trebolazabala, M. Maguregui, H. Morillas, A. de Diego, and J. M. Madariaga, "Portable Raman spectroscopy for an in-situ monitoring the ripening of tomato (Solanum lycopersicum) fruits," *Spectrochim. Acta Part A Mol. Biomol. Spectrosc.*, vol. 180, pp. 138–143, 2017.

[48] X. Hu, Q. Cai, Y. Fan, T. Ye, Y. Cao, and C. Guo, "Molecularly imprinted polymer coated solid-phase microextraction fibers for determination of Sudan I–IV dyes in hot chili powder and poultry feed samples," *J. Chromatogr. A*, vol. 1219, pp. 39–46, 2012.

[49] A. Saroj, V. Ramanathan, "Bismuth oxybromide based novel substrate for surface enhanced Raman spectroscopy." *Vibrational Spectroscopy*, vol.124, pp.103463, 2023.

[50] G. R. Ferreira, H. C. Garcia, M. R. C. Couri, H. F. Dos Santos, and L. F. C. de Oliveira, "On the azo/hydrazo equilibrium in Sudan I azo dye derivatives," *J. Phys. Chem. A*, vol. 117, no. 3, pp. 642–649, 2013.